REPORT DOCUMENTATION PAGE

Form Approved OMB NO. 0704-0188

1. REPORT DATE (DD-MM-YYYY)	2. REPORT TYPE	3. DATES COVERED (From - To)
18-04-2018	Final Report	1-Oct-2012 - 31-Dec-2017

4. TITLE AND SUBTITLE
Final Report: Single-crystal fiber lasers

5a. CONTRACT NUMBER
W911NF-12-1-0536

5b. GRANT NUMBER

5c. PROGRAM ELEMENT NUMBER

6. AUTHORS

5d. PROJECT NUMBER

5e. TASK NUMBER

5f. WORK UNIT NUMBER

7. PERFORMING ORGANIZATION NAMES AND ADDRESSES

Rutgers, The State University of New Jersey
3 Rutgers Plaza
ASB III, 2nd Floor
New Brunswick, NJ 08901 -8559

8. PERFORMING ORGANIZATION REPORT NUMBER

9. SPONSORING/MONITORING AGENCY NAME(S) AND ADDRESS (ES)

U.S. Army Research Office
P.O. Box 12211
Research Triangle Park, NC 27709-2211

10. SPONSOR/MONITOR'S ACRONYM(S)
ARO

11. SPONSOR/MONITOR'S REPORT NUMBER(S)
62114-PH-HEL.20

12. DISTRIBUTION AVAILIBILITY STATEMENT

Approved for public release; distribution is unlimited.

13. SUPPLEMENTARY NOTES

The views, opinions and/or findings contained in this report are those of the author(s) and should not contrued as an official Department of the Army position, policy or decision, unless so designated by other documentation.

14. ABSTRACT

15. SUBJECT TERMS

16. SECURITY CLASSIFICATION OF:			17. LIMITATION OF ABSTRACT	15. NUMBER OF PAGES	19a. NAME OF RESPONSIBLE PERSON
a. REPORT	b. ABSTRACT	c. THIS PAGE			James Harrington
UU	UU	UU	UU		19b. TELEPHONE NUMBER 732-445-3932

RPPR Final Report
as of 10-Jul-2018

Agency Code:

Proposal Number: 62114PHHEL **Agreement Number: W911NF-12-1-0536**
INVESTIGATOR(S):

Name: James A. Harrington
Email: jaharrin@rutgers.edu
Phone Number: 7324453932
Principal: Y

Organization: **Rutgers, The State University of New Jersey - New Brunswick**
Address: 3 Rutgers Plaza, New Brunswick, NJ 089018559
Country: USA
DUNS Number: 001912864 EIN: 226001086
Report Date: 31-Mar-2018 Date Received: 18-Apr-2018
Final Report for Period Beginning 01-Oct-2012 and Ending 31-Dec-2017
Title: Single-crystal fiber lasers
Begin Performance Period: 01-Oct-2012 **End Performance Period:** 31-Dec-2017
Report Term: 0-Other
Submitted By: James Harrington Email: jaharrin@rutgers.edu
Phone: (732) 445-3932

STEM Degrees: 19 **STEM Participants:** 19

Major Goals: Essentially all fiber lasers in use today are made of glass. These glass structures normally involve a double-clad structure in which the core glass has been doped with a variety of rare-earth ions notably ytterbium which yields ytterbium-doped fiber lasers (YDFL). Yet there are some limitations to power scaling of glass fiber lasers which result from laser induced damage to the small cores, nonlinear effects such as stimulated Brillouin scattering (SBS), and thermal loading. The goal of this research is to develop a new and novel class of high power fiber lasers based on crystalline materials rather than the conventional glass fiber structure. The basic premise of this work is the rather straightforward idea that crystalline host materials such as YAG and other garnets are known to deliver extremely high laser powers. The technology of Nd:YAG lasers employing conventional rods and disks is well established and reliable. The intent of this work is to draw from the broad knowledge base for solid-state lasers, eg. Nd:YAG, to extend this technology to fabricate single-crystal (SC) fiber lasers. SC fiber lasers would be scalable to much higher power levels compared to their glass counterpart largely because SC fiber lasers have a significantly higher thermal conductivity and also much higher thresholds for nonlinear processes such as SBS. In fact, theoretical calculations predict that the SBS threshold for YAG is as much as 1,000 times greater than that of silica. Simply put, this implies that SC YAG fibers should deliver over 6 kW to as much as 30kW per fiber compared to about 1.5 kW for silica fiber lasers. The impact of SC fiber lasers with the potential to perform in a manner analogous to the proven capabilities for the bulk crystalline oxide lasers would be a significant improvement in the current DoD arsenal of glass fiber lasers.

The approach used to fabricate SC fibers is Laser Heated Pedestal Growth (LHPG). In this well-established technique, the tip of a doped-oxide host preform, for example, Er3+ in YAG, is melted with a CO2 laser and an SC fiber is pulled from the molten oxide. A major part of this effort is to devise a method to clad the SC fibers. There are basically two methods that can be used to clad the fiber. The most desirable is to clad the fiber as it is grown using a rod-in-tube method in which we start with a core/clad preform to produce a graded-index cladding. An alternative approach is to grow very small diameter, < 50 ?m, fibers and then apply a cladding to the small diameter fiber. The SC fibers are characterized using optical spectroscopy and fluorescence imaging. Modeling of the SC fiber refractive index profiles, fiber structure, and thermal properties as well as lasing parameters are being done to help guide the selection of materials needed to make a true fiber laser. Finally, the lasing properties of the SC fibers are measured.

Accomplishments: 1. Grew SC fibers from rare-earth doped oxides using the technique of laser heated pedestal growth (LHPG). SC fibers grown to date include Er3+, Ho3+, Yb, and Tm3+ doped YAG in diameters from 100 to 300 microns and lengths up to 100 cm.
2. Major improvements were made in the LHPG apparatus mostly through the use of a double transmission

axicon system in contrast to the reflective system used by most investigators.
3. An important part of this research is cladding the YAG fibers. We have used the rod-in-tube method to grow SC fibers with a pure YAG clad surrounding an Er:YAG core. The index profiling measurements of this rod-in-tube method indicate that there is a gradient in the Er-ion concentrations with more Er ions in the center than at the edge. These results offer a promising path to producing clad fibers as the fiber is grown in contrast to alternative post-cladding methods.
4. A new method of introducing rare-earth dopants into YAG fiber was developed; This method involved using sol-gel coatings containing rare-earth dopants that were applied to the 330-micron diameter fiber and then regrown into smaller diameters.
5. Lowered the total loss in the pure and doped to less than 0.1 dB/m. This is a 10-fold decrease in loss from a year ago. It is also to our knowledge the lowest loss measured for any SC YAG fiber.
6. Fluorescence measurements of the YAG clad/Er:YAG SC fibers have been made and correlated with the index profiling data of these fibers.
7. The spontaneous emission spectra of 0.5% Er:YAG, 0.5% Ho:YAG fibers have been obtained and the potential pumping wavelengths and laser lines identified.
8. Small signal gain measurements were performed, demonstrating the fiber-like characteristics of the SC fibers.
9. Lasing in 0.5% Ho:YAG SC fibers was obtained from a 11-cm long 330-micron diameter fiber. The slope efficiency of 72.3% is the highest slope efficiency ever obtained for a RE-doped SC fiber. See Ref. 15 for summary of this work.

Training Opportunities: Nothing to Report

Results Dissemination: Some samples of SC doped and undoped YAG fibers supplied to various interested parties during this program. See Tech Transfer for details.

Honors and Awards: 1. James A Harrington, PI - received the 2014 Gold Medal of SPIE the highest honor awarded by this professional society for optical engineering.

2. Wesley Kendall, undergrad at Rutgers received an NSF Fellowship for his graduate training starting next year at Duke University.

3. S.C. Rand, Distinguished Speaker, Indian Institute of Technology Kharagpur (2014)

4. S.C. Rand, Erskine Fellow, University of Canterbury NZ (2014)

5. S.C. Rand, APS-IUSSTF-Professorship (2013)

6. S.C. Rand, OSA Travel Fellowship (2013)

7. E.F.C. Dreyer, NSF Fellowship (2013-2018)

8. A. C. Mendes, CNPQ Brazilian Study Abroad Scholarship (2016)

Protocol Activity Status:

Technology Transfer: Supplied single-crystal doped and undoped YAG to the government (SPAWAR-Ramesh Shori) and Chance Carter at LLNL. Also samples of Yb:YAG fibers sent to Stephen McCahon, Applied Optical Sciences, Tucson, AZ.

PARTICIPANTS:

Participant Type: PD/PI
Participant: James A Harrington
Person Months Worked: 3.00 **Funding Support:**
Project Contribution:
International Collaboration:
International Travel:
National Academy Member: N

Other Collaborators:

Participant Type: Co PD/PI
Participant: Eric Johnson
Person Months Worked: 2.00 **Funding Support:**
Project Contribution:
International Collaboration:
International Travel:
National Academy Member: N
Other Collaborators:

Participant Type: Co PD/PI
Participant: Stephen Rand
Person Months Worked: 2.00 **Funding Support:**
Project Contribution:
International Collaboration:
International Travel:
National Academy Member: N
Other Collaborators:

Participant Type: Staff Scientist (doctoral level)
Participant: Keith Miller
Person Months Worked: 6.00 **Funding Support:**
Project Contribution:
International Collaboration:
International Travel:
National Academy Member: N
Other Collaborators:

ARTICLES:

Publication Type: Journal Article Peer Reviewed: Y **Publication Status:** 1-Published
Journal: Optics Express
Publication Identifier Type: DOI Publication Identifier: 10.1364/OE.22.014896
Volume: 22 Issue: 12 First Page #: 0
Date Submitted: Date Published:
Publication Location:
Article Title: Ho:YAG single crystal fiber: fabrication and optical characterization
Authors:
Keywords: Rare-earth materials, fiber lasers, single-crystal fiber optics
Abstract: 0.5% Holmium (Ho) doped YAG single crystal fiber (SCF) was fabricated using Laser Heated Pedestal Growth (LHPG) method and characterized for its optical absorption and emission properties involving transitions between the 5I8 and 5I7 energy levels. The results verified the absorption peaks suitable for in-band direct pumping at 1908 nm and 1932 nm with the emission occurring between 2050 and 2150 nm. Small signal gain measurements were also performed for demonstrating the fiber like characteristics of the SCF.
Distribution Statement: 1-Approved for public release; distribution is unlimited.
Acknowledged Federal Support:

CONFERENCE PAPERS:

RPPR Final Report
as of 10-Jul-2018

Publication Type: Conference Paper or Presentation **Publication Status:** 1-Published
Conference Name: SPIE LASE
Date Received: 26-Aug-2016 Conference Date: 15-Jan-2015 Date Published: 28-Feb-2015
Conference Location: San Francisco, California, United States
Paper Title: Single-crystal fiber optics: a review
Authors: James A Harrington
Acknowledged Federal Support: **Y**

Publication Type: Conference Paper or Presentation **Publication Status:** 1-Published
Conference Name: SPIE LASE
Date Received: 16-Apr-2018 Conference Date: 12-Feb-2018 Date Published: 20-Feb-2015
Conference Location: San Francisco, California, United States
Paper Title: Erbium distribution in single crystal YAG fibers grown by laser-heated pedestal growth technique
Authors: c nie, s bera, j melzer, j harrington, e dreyer, s rand, s t-reichert, c hoef
Acknowledged Federal Support: **Y**

Publication Type: Conference Paper or Presentation **Publication Status:** 1-Published
Conference Name: SPIE LASE
Date Received: 19-Aug-2016 Conference Date: 13-Feb-2016 Date Published:
Conference Location: San Francisco, California, United States
Paper Title: Cladding single crystal YAG fibers grown by laser heated pedestal growth
Authors: Subhabrata Bera, Craig D. Nie, James A. Harrington, Theresa Chick, Ayan Chakrabarty, Stephen Treml
Acknowledged Federal Support: **Y**

Publication Type: Conference Paper or Presentation **Publication Status:** 1-Published
Conference Name: Photonics West, Solid State Lasers XXVI
Date Received: 26-Aug-2016 Conference Date: 26-Jan-2014 Date Published: 20-Feb-2015
Conference Location: San Francisco, CA
Paper Title: Investigation of the amplification properties of Ho:YAG single crystal fiber
Authors: Yuan Li, Zeyu Zhang, Ian Buckley, Jerome K. Miller, Eric G. Johnson, Craig D. Nie, James A. Harrington
Acknowledged Federal Support: **Y**

Publication Type: Conference Paper or Presentation **Publication Status:** 1-Published
Conference Name: SPIE LASE
Date Received: 16-Apr-2018 Conference Date: 28-Feb-2018 Date Published: 22-Mar-2018
Conference Location: San Francisco, California, United States
Paper Title: Single-crystal rare-earth doped YAG fiber lasers grown by the laser-heated pedestal growth technique
Authors: James Harrington, Craig Nie, Elizabeth Cloos, Stephen Rand, Yuan Li, Eric Johnson
Acknowledged Federal Support: **Y**

DISSERTATIONS:

Publication Type: Thesis or Dissertation
Institution: Clemson University
Date Received: Completion Date: 12/15/16 12:00AM
Title: Study on the amplification of spatial modes in a crystal rod amplifier
Authors: Yuan, Li
Acknowledged Federal Support: **Y**

RPPR Final Report
as of 10-Jul-2018

Publication Type: Thesis or Dissertation
Institution: Rutgers University
Date Received: 17-Apr-2018 Completion Date: 1/12/17 5:00AM
Title: Rare-earth-doped single-crystal YAG fibers grown by the laser heated pedestal growth technique
Authors: Craig, Nie
Acknowledged Federal Support: **Y**

Final Technical Report

October 1, 2012 through December 31, 2017

Table of Contents

Abstract

This research is designed to model, fabricate, and characterize rare-earth (RE) doped, single-crystal (SC) fibers for the use as high power lasers and amplifiers. The basic concept behind this research program is to take advantage of the high power capability of RE-doped oxide crystals to fabricate SC fibers that have the potential of exceeding the output of glass fiber lasers used today. Specifically, SC fiber lasers would be scalable to much higher power levels compared to their glass counterpart largely because SC fibers, made from such materials as RE-doped YAG,

have a significantly higher thermal conductivity and, most importantly, higher thresholds for the onset of stimulated Brillouin scattering (SBS)[1]. The basic approach is to grow SC fibers from RE-doped oxides using the technique of laser heated pedestal growth (LHPG). SC fibers grown to date include Er^{3+}, Ho^{3+}, Tm^{3+}, Yb^{3+}, and Nd^{3+} doped YAG in diameters from 100 to 300 microns and lengths up to 110 cm. The spontaneous emission spectra of 0.5% Er:YAG, 0.5% and 4% Ho:YAG, and 6% Tm:YAG fibers have been obtained and the potential pumping wavelengths and laser lines identified. Most recently we have concentrated on studying the optical absorption and emission properties of 0.5% Ho:YAG for transitions between the $^5I_8$ and $^5I_7$ energy levels. These results verified the absorption peaks suitable for in-band direct pumping at 1908 nm and 1932 nm with the emission occurring between 2050-2150 nm. Small signal gain measurements were performed and we did achieve lasing in one 10.5 cm long Ho:YAG SC fiber sample. This SC Ho-doped YAG fiber gave a slope efficiency of 72.3% which is close to that measured in the bulk Ho-doped YAG samples (~80%). To our knowledge this is the highest slope efficiency measured for a RE-doped YAG fiber. An important part of this research is cladding the YAG fibers. We have used several techniques to clad the fibers. One method that we have used is the rod-in-tube (RIT) method to grow SC fibers with a pure YAG clad surrounding an Er:YAG core. The index profiling measurements of this rod-in-tube method indicate that there is a gradient in the Er-ion concentrations with more Er ions in the center than at the edge. We also see a gradient of Nd ions in YAG fibers but the difference is that the Nd:YAG fibers were not grown from a rod-in-tube preform rather they were grown for a single Nd:YAG source. The Nd ion is larger than the Y ions they replace so there is a natural grading of the Nd ions with more in the center than the outside. We feel that we may use this observation as a future means to achieve a cladding in the fibers. Finally, we have used a sol-gel method to coat both the preform YAG rods and for the fiber itself. These results offer a promising path to producing clad fibers as the fiber is grown in contrast to alternative post-cladding methods. Future plans include further cladding studies of SC fibers, including a look at the deposition of a crystalline YAG clad via hydrothermal methods, further index profiling, and pumping the doped YAG fibers to achieve higher laser power in the wavelength range between 1600 to 2100 nm.

Scientific Progress and Accomplishments

Overall Program Objectives and Background

Essentially all fiber lasers in use today are made of glass. These glass structures normally involve a double-clad structure in which the core glass has been doped with a variety of rare-earth ions notably ytterbium which yields ytterbium-doped fiber lasers (YDFL). Yet there are some limitations to power scaling of glass fiber lasers which result from laser induced damage to the small cores, nonlinear effects such as stimulated Brillouin scattering (SBS), and thermal loading. The goal of this research is to develop a new and novel class of high power fiber lasers based on crystalline materials rather than the conventional glass fiber structure. The basic premise of this work is the rather straightforward idea that crystalline host materials such as YAG and other garnets are known to deliver extremely high laser powers. The technology of Nd:YAG lasers employing conventional rods and disks is well established and reliable. The intent of this work is to draw from the broad knowledge base for solid-state lasers, eg. Nd:YAG, to extend this technology to fabricate single-crystal (SC) fiber lasers. SC fiber lasers would be scalable to much higher power levels compared to their glass counterpart largely because SC fiber lasers have a

significantly higher thermal conductivity and also much higher thresholds for nonlinear processes such as SBS. In fact, theoretical calculations predict that the SBS threshold for YAG is as much as 1,000 times greater than that of silica. Simply put, this implies that SC YAG fibers should deliver over 6 kW to as much as 30kW per fiber compared to about 1.5 kW for silica fiber lasers[1]. The impact of SC fiber lasers with the potential to perform in a manner analogous to the proven capabilities for the bulk crystalline oxide lasers would be a significant improvement in the current DoD arsenal of glass fiber lasers.

The approach used to fabricate SC fibers is Laser Heated Pedestal Growth (LHPG)[2]. In this well-established technique, the tip of a doped-oxide host preform, for example, Er^{3+} in YAG, is melted with a CO_2 laser and an SC fiber is pulled from the molten oxide. A major part of this effort is to devise a method to clad the SC fibers. There are basically two methods that can be used to clad the fiber. The most desirable is to clad the fiber as it is grown using a rod-in-tube method in which we start with a core/clad preform to produce a graded-index cladding. An alternative approach is to grow very small diameter, < 50 μm, fibers and then apply a cladding to the small diameter fiber. The SC fibers are characterized using optical spectroscopy and fluorescence imaging. Modeling of the SC fiber refractive index profiles, fiber structure, and thermal properties as well as lasing parameters are being done to help guide the selection of materials needed to make a true fiber laser. Finally, the lasing properties of the SC fibers are measured.

Key accomplishments of the program

Dramatic reduction in loss of SC YAG fiber optics – Rutgers University

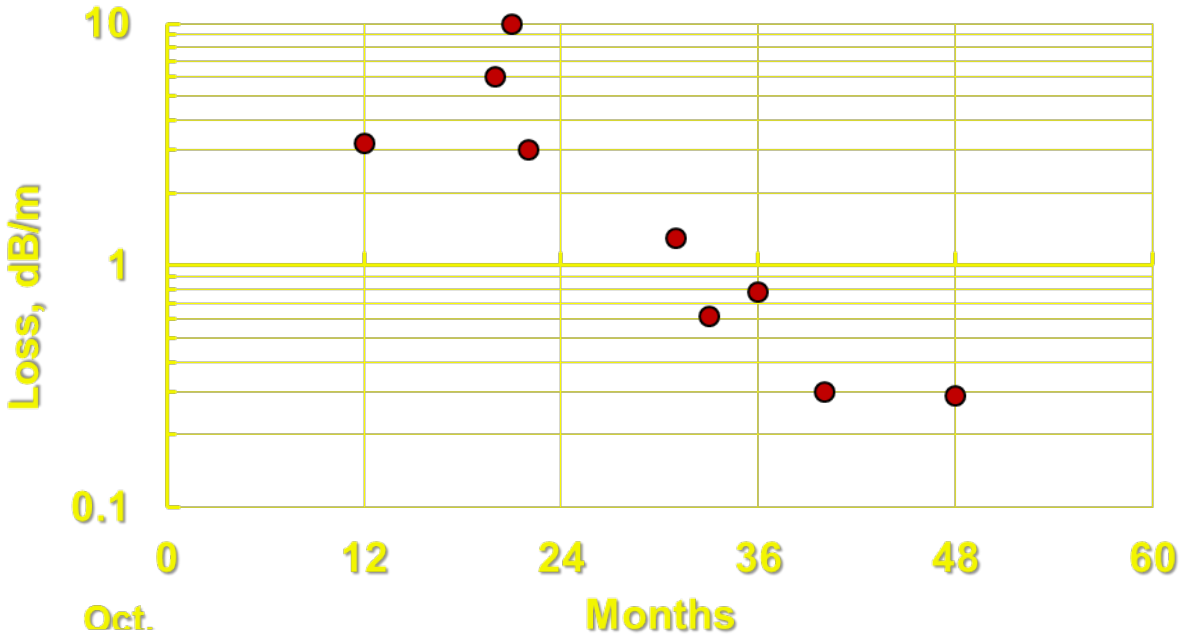

Figure 1 Reduction in SC fiber loss over program timeline.

An obvious major goal of any program designed to fabricate crystalline fiber optics is to reduce the overall attenuation in the fibers. When we began this program in the fall of 2012, the losses in our YAG fibers were as high as 10 dB/m at 1 μm. This is an untenable loss for any application involving the use of these fibers as amplifiers or lasers. From the time graph in Fig. 1 we see that the losses were reduced by a factor of almost 100 by the end of the program. The losses that we obtained in our YAG fibers are the lowest ever obtained for YAG fiber optics and, in fact are lower than the lowest losses measured for SC sapphire fiber. Specifically, the most recent results have yielded a loss at 1 μm less than 0.2 dB/m. We feel that this loss is well below the losses required for the operation of m-long lengths of fiber required for active laser applications.

Evidence of gradient refractive index in Er-doped YAG fibers optics – Rutgers and University of Michigan

A major challenge in this program from the outset was finding methods to apply a cladding to crystalline fibers in essentially the same manner as glass fibers. In glass, the refractive index of the cladding may be lowered to ensure guided wave propagation through total internal reflection. Unfortunately, whereas glass can be heated to flow like a liquid while preserving the waveguiding properties, crystals do not have a glass forming region and cannot be drawn into fibers directly at all. Hence the focus of this research effort was to discover a method for cladding crystalline fibers to ensure waveguiding, and research at the University of Michigan was to characterize their dopant distributions for laser applications.

We found that growing YAG fibers from YAG crystals heavily doped with Er ions led to an SC fiber with a radial index profile revealing that there more Er ions in the core than in the outer

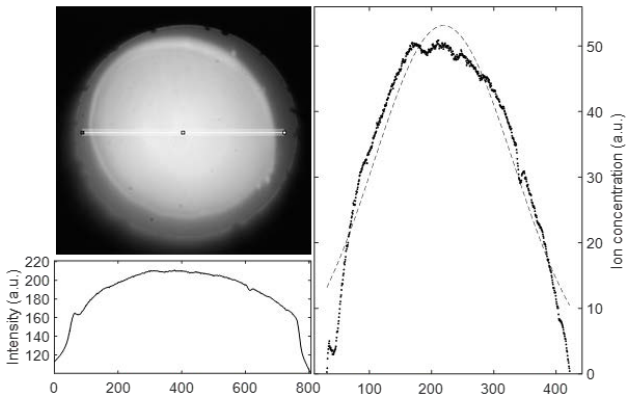

Figure 2 - Er^{3+} distribution in 50% Er^{3+}:YAG core with pure YAG cladding grown at 1 mm/min. The profiles are one-dimensional lineouts through fluorescent images giving dopant concentration versus position across each fiber sample.

regions of the fiber. The fluorescence mapping data of one such Er-doped YAG fiber is shown in Fig. 2. The fluorescence was scanned across the diameter and we can see from the fluorescence of the Er ions that there are more Er ions in the center than at the edges of the fiber. This important result has led us to investigate other RE ions, such as Nd^{3+}, which may be used to ultimately grad the index of the fiber and to achieve waveguiding.

Lasing in Er-doped YAG fibers optics – Rutgers and Clemson University

Lasing was demonstrated for the first time at 2.09 μm in 0.5% Holmium (Ho) doped YAG single crystal fiber (SCF) fabricated using the Laser Heated Pedestal Growth (LHPG) method. Output power of 23.5 W with 67.5% optical-to-optical slope efficiency is, to the best of our knowledge, the highest output power achieved at 2 μm from a SCF fabricated using LHPG. With continued improvement in the quality of the SCF and better thermal management, output power of few 100s W and higher, especially in the 2 μm spectral region, is realizable in the very near future.

The work at Clemson using the Rutgers LHPG grown 0.5% Ho:YAG SCF, 320 μm diameter and 115 mm long, were used for the lasing experiments. This length to diameter ratio ensures that multiple bounces are realized and that the SCF is actually guiding the pump and signal beams with the fiber geometry. Recent improvements in the LHPG fabrication process have led to significant reduction in transmission losses within the SCF loss lowered from 8.7 dB/m to approximately 1.3 dB/m at 2.0 μm in this work. With continued improvements in the SCF transmission and recent advances in the ability to clad the SCF, power scaling the laser output to few hundred watts in the 2 μm spectral region should be possible. The data in Fig. 3 show the results of the pumping experiments and the measured slope efficiency.

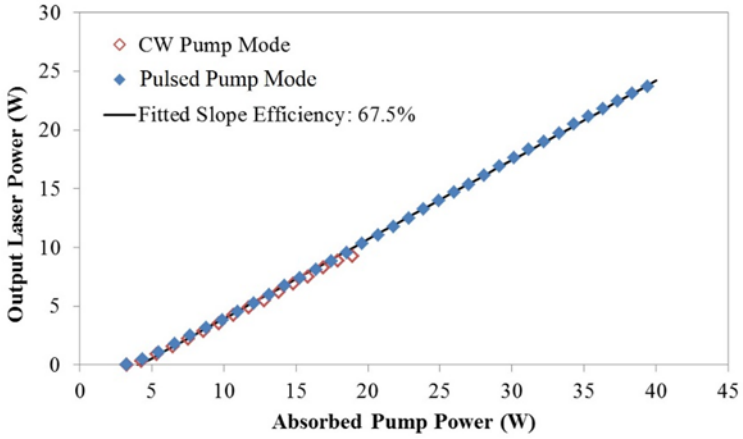

Fig. 3. The output laser power as a function of absorbed pump power under both CW and pulsed pump mode.

Growth, cladding, and optical loss measurements of SC fibers – Rutgers University

SC fibers have been grown by several methods, including Edge-Defined Film Fed Growth (EFG)[3], micro-pulling-down[4], and the LHPG method[2]. The most common method used today is LHPG. This method was first developed by Haggerty[5] at MIT and then further refined by a number of researchers including those at Stanford University[6], Rutgers University[2], University of South Florida[7], Shasta Crystals, Inc.[8], and others[9]. LHPG is a crucibleless method much like the float zone technique. In the LHPG technique, we begin by melting the tip of a 1-mm diameter ceramic or rare-earth doped SC YAG source rod with a CO_2 laser. The YAG

source rod is seeded with a YAG fiber or a Pt-Rh wire and an SC fiber is pulled from the molten oxide. Figure 4 shows a sketch of the LHPG apparatus. The SC fibers that we have grown to date are as long as 60 cm with diameters ranging from 120 to 330 μm. The fibers grown from most of the preforms are unclad. The SC fibers that we have grown to date include, pure YAG, 0.5% and 50% Er:YAG, 0.5%, 1%, and 4% Ho:YAG, 6% Tm:YAG, 2.5% Nd:YAG, and 0.25% Yb:YAG. The longest length of doped YAG fiber has been about 100 cm.

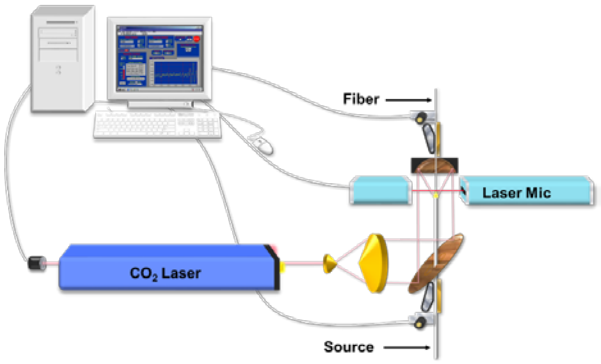

Fig. 4 - Experimental set-up of the LHPG technique used to grow SC YAG fibers. The use of transmissive axicons rather than a reflective optics allows us more flexibility in adjusting the optical parameters of the ring of CO_2 laser light.

A unique improvement of our LHPG apparatus is the use of a pair of AR-coated ZnSe axicons to convert the Gaussian CO_2 laser beam into a ring, rather than the more common method employing a reflective (refraxicon) focusing system [6, 10, 11]. The growth speed is between 1 to 4 mm/min and the source-to-fiber reduction for stable growth is about 3:1. Almost all of our starting source material is single-crystal YAG with dimensions 1 x 1 x 120 mm. The 25 W CO_2 laser is amplitude stabilized by taking a small power from the rear output mirror and inputting this signal to a LabView program. This program returns a signal to the power supply to control the power to $\pm$0.2%. In addition to amplitude stabilization, we also use a laser micrometer to measure and control the fiber diameter.

Losses in SC fibers – see recent publication for more details for this section cf. Ref. 2

1. Spectral losses

One of the most important aspects of any fiber development program is a thorough understanding of the losses in the fibers. During this past year we have concentrated on the measurement of the total and scattering losses in our YAG fibers. In particular, we have made very accurate loss measurements for fibers grown from several different crystal suppliers and for fibers grown under quite different growth parameters such as pulling speed, temperature, and fiber diameter. A significant accomplishment this year was the reduction of the total loss to a level of less than 0.1 dB/m at 1064 nm. This is by far the lowest loss YAG fiber ever made.

The total loss for undoped YAG SC fibers with a diameter of about 330 μm was measured from 530 to 1064 nm using a series of lasers. These measurements had to be done very carefully as the fibers were generally less than a meter in length. In Fig. 5, we show the data at the different laser wavelengths for different starting host material. There were two main suppliers of our YAG bars. One source was a Chinese silicon foundry that also grew YAG crystals. The other source was Scientific Materials, Bozeman, MT. The Scientific Materials was available in

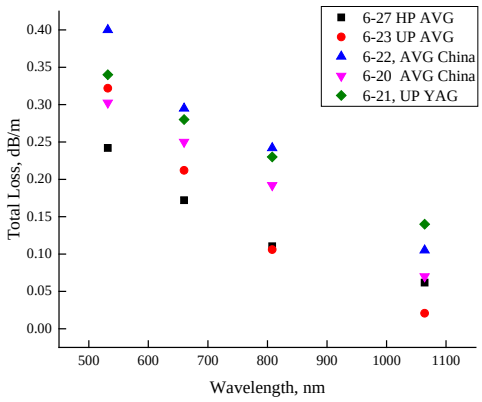

Fig. 5 – Total SC fiber loss for different starting materials. Note the extremely low loss at 1.06 μm for the ultrapure material from Scientific Materials, Inc.

several grades, UP (ultra pure) and HP (high purity). According to Scientific Materials the UP material involves an extra step of purification. Looking at the data in Fig. 5 we see that the UP material does exhibit the lowest loss with the loss at 1064 nm less than 0.05 dB/m. As mentioned above, this is the lowest loss ever measured for an undoped YAG fiber and, it should be pointed out, is orders of magnitude less than when the program started 5 years ago and the fiber losses were at best 4 dB/m at 1064 nm.

The other optical measurement was a separate measurement of the scattering losses for the same undoped fibers. We began studying the scattering losses several years ago as a means to better understand the contribution of scattering to the total loss in the fibers. In Fig. 6 the lowest measured scattering losses are shown for the pure YAG fibers at the same laser wavelengths given in Fig. 5 for the total loss. Again, we note that the UP material from Scientific Materials

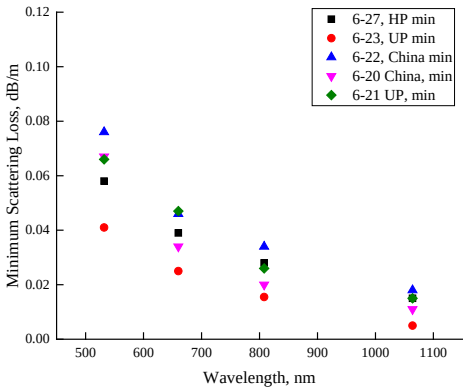

Figure 6 – Scattering losses for the same fibers given in Fig. 5. Again note the very low scattering at 1.06 μm.

exhibits the lowest scattering. In general, scattering losses are contribute about

30% to the total loss.

2. Optimizing alignment and growth of low-loss YAG SC fiber or how we achieved the very low loss in SC YAG fiber optics

During the final year of this program there was a concentrated effort on lowering the loss of the fibers by making a critical analysis of our LHPG parameters. In large part this involved developing methods that would enable us to accurately align the laser beam so that it was perfectly symmetric on the YAG source rod. This work has recently been published in Applied Optics. In this work each optical component of the LHPG system was slightly misaligned and then re-aligned to achieve a symmetric melt zone at the tip of the YAG rod.

The quality of the SC fibers grown using the LHPG method depends largely on the symmetrical shape and homogeneity of the melt zone. Asymmetric heating in the melt leads to highly strained fibers of poor optical quality fibers which are characterized by high transmission losses. Moreover, a non-uniform distribution of heat in the melt leads to curved fibers which, very often, jam inside the fiber pulling mechanism and stop growing altogether. Hence, proper alignment of optical components is central to the growth process. However, conventional aligning techniques for visible and near-IR lasers are not applicable in this situation, as the 10.6 μm CO_2 laser is in the mid-IR wavelength region. This means that typical IR visualization and alignment cards do not work. Moreover, effects of different misalignment are difficult to distinguish using carbon paper or imaging plates. Hence the effects of misalignments of each of the optical components, which cause asymmetric heating of the melt, were simulated using Zemax, a commercially available optical ray-tracing software. By isolating the misalignments causing the non-uniformity in the melt zone, it was possible to fine-tune the optical alignment of the components. The fiber growth of 120 μm fibers was much more susceptible to misalignments than the growth of 330 μm fibers. In the case of the larger diameter fibers, the CO_2 laser beam needed to be focused to a 1 mm spot size compared to the 340 μm spot size, therefore requiring higher tolerances for alignment.

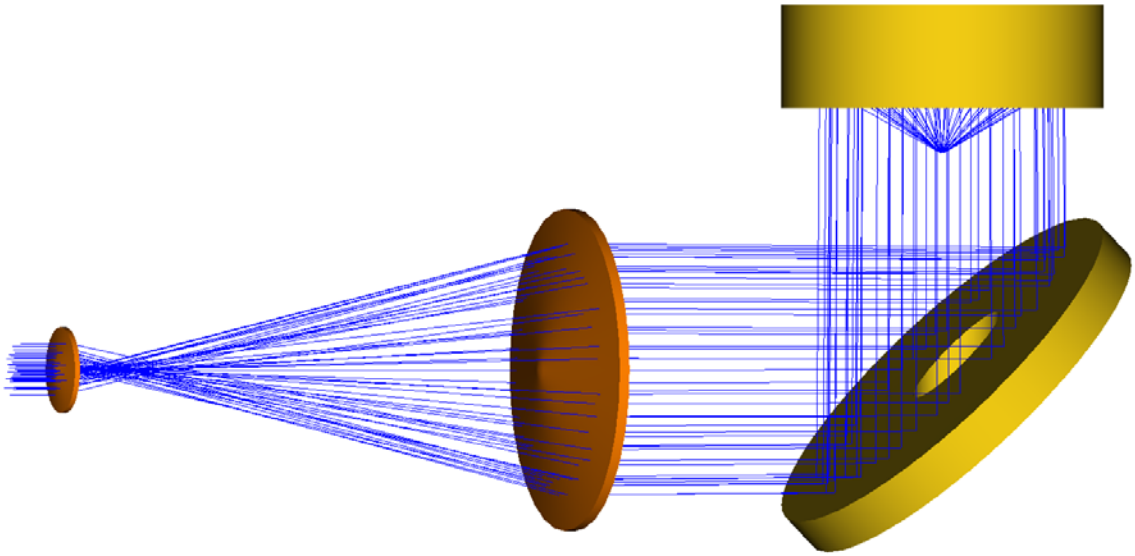

Figure 7 - The primary optical components in the LHPG apparatus. These four components transform the Gaussian beam from the CO_2 laser to form a ring and then focus it on top of a source bar.

In the system shown in Fig. 7, a relatively large diameter (~7 mm $1/e^2$) CO_2 laser beam is incident on a 28 mm diameter zinc selenide (ZnSe) axicon with an apex angle of 10°. This first axicon produces a region of focused light, which is well known in optical literature for use in producing non-diffracting beams known as Bessel beams. However, past this region, the light diverges to a ring. Following the first axicon, 120 mm away, is a second ZnSe axicon with the same apex angle. The diverging ring is collimated by this second, larger ZnSe axicon. Both of the axicons have an anti-reflective (AR) coating for 10.6 µm laser radiation. Following the two axicons, a 45° gold coated flat mirror turns the light upwards. Finally, the ring is focused to a point using a 25.4 mm focal length gold-coated parabolic mirror.

Two axicons, a turning mirror, and an on-axis parabola define the optical system in its simplest form. The simulations look primarily at the alignment of the two axicons. By way of example, we show in Fig. 8 just one of the misalignments resulting from the simulations. An input Gaussian beam is used for all of the simulations. For Fig. 8, the first column is the cross-section seen 35 mm after the edge of the second axicon in the two-axicon beam shaping system. This will always look close in shape to a ring. However, the farther that the imaging plane is set, the more the error in the axicon alignment can be seen. The second column contains the imaging plane roughly 1 mm before the focus. The shape and intensity of the ring output looks appreciably altered by shifts in the first axicon. This is expected, as the axicon being shifted indicates that the Gaussian beam is off-center from the axicon tip. The axicon's circular symmetric conical shape is what causes the diverging ring shape, and therefore the case of a non-concentric beam and axicon leads to a non-uniform ring distribution at the output.

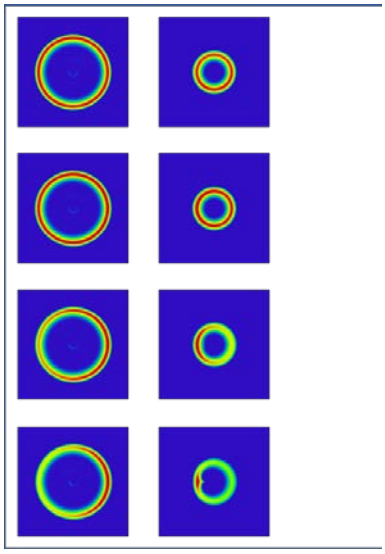

Figure 8 - Effect of lateral displacement of first axicon. The first column is the cross-section 35 mm after the second axicon. The second column is the imaging plane slightly above the focus.

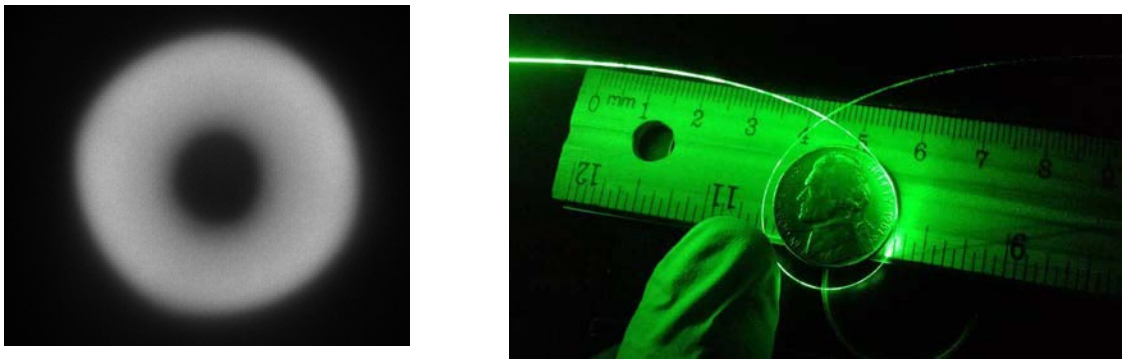

Figure 9 - Photograph of symmetric focus achieved on a 340 µm source by fine-tuning alignment of components. A 120 µm diameter SC YAG fiber demonstrating coilability

In a previous work, we published, to our knowledge, the lowest loss for SC YAG fibers [2]. The diameter of the fibers studied in that work was about 340 µm. In this work, we have been able to replicate comparable results for 120 µm fibers. Growing low-loss coilable fiber is more involved, as this requires much better alignment of the optical components to obtain a more uniform focus of the CO_2 laser beam. The improvements in alignment were assisted by the results obtained from the simulations using the optical ray-tracing software described above. We believe that the improved alignment led to the reduction of crystal strain and defects caused by non-uniform heating in the melt. Non-uniform heating leads to a non-uniform growth surface of the crystal which introduces crystal strain and defects such as dislocations, slip planes, etc. These degrade the quality of the crystal fiber waveguides and contribute to the transmission losses in the fibers. Using improved alignment of optical components, attenuation losses have been reduced from about 10 dB/m to less than 1 dB/m. To date, the lowest measured loss for a 120 µm diameter YAG SC fiber at 1064 nm is 0.5 dB/m. The attenuation losses measured at different wavelengths

in a different 30 cm long, 120 µm diameter YAG SC fiber is shown in Figure 10. The figure shows an increasing total attenuation loss in the fiber with decreasing wavelength. The increase in total attenuation losses in the fiber with decreasing wavelength is mostly due to increased scattering losses. The losses appear to have a $\lambda^{-2.4}$ dependence on wavelength.

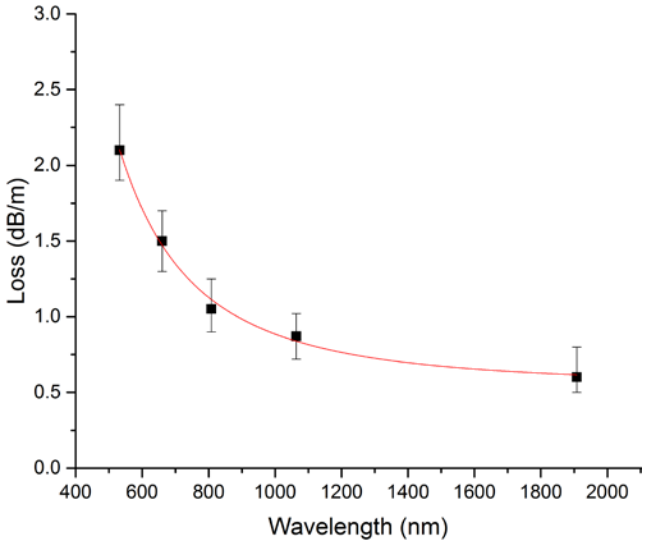

Figure 10 - Total attenuation losses for a 30-cm long 120 µm diameter YAG SC fiber at different wavelengths

3. Growth and lasing of single crystal YAG fibers with different Ho^{3+} concentrations

This part of the research program was a collaboration between Rutgers where the Ho-doped YAG fibers were grown and Clemson where the lasing measurements were made. The basic idea was to devise a method to grow single crystal (SC) yttrium aluminum garnet (YAG) fibers with varied rare-earth ion dopant concentrations. Crystalline holmium aluminum garnet (HoAG), prepared via sol-gel process, was dip-coated on to previously grown SC YAG fibers. The HoAG coated SC YAG fiber preforms were then regrown to a smaller diameter using our LHPG apparatus. The final dopant concentration of the regrown SC fiber was varied by changing the number of HoAG coatings on the preform. SC Ho:YAG fibers, 120 µm diameter, with four different dopant concentrations were grown. Lasing was demonstrated at 2.09 µm for these fibers. A maximum of 58.5% optical-to-optical slope efficiency was obtained.

Sol-gel based synthesis of rare-earth aluminum garnets has been previously studied by using an acetate-glycolate pathway by Dubnikova et al[12]. In this study, we use a similar method to obtain polycrystalline HoAG. HoAG is derived by the hydrolysis and condensation of holmium oxide and aluminum nitrate. The materials used for the synthesis were Ho_2O_3 (Alfa Aeser, 99.995%), $Al(NO_3)_3\ 9H_2O$ (Acros Organics, 99+%), glacial CH_3COOH (Fisher Scientific) and ethane-1,2-diol ($(-CH_2OH)_2$) (Acros Organics). Holmium oxide is refluxed in 0.02 M acetic acid at 60-70°C for 6-8 hours to obtain holmium acetate. Aluminum nitrate was added to the solution and the solution was constantly stirred at 70°C for 2-3 hours. Finally, ethyl glycolate is added and the final solution is kept at the same temperature, slowly evaporating the dissolved water to raise the viscosity of the precursor sol. Although the viscosity is allowed to increase considerably, gelation is not reached. The subsequent sol was used for dip coating.

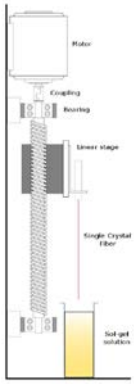

Figure 11 - Schematic of dip-coating set-up

The HoAG sol was applied to a SC YAG fiber with a diameter of 335 µm, using a dip-coater illustrated in Fig. 11. Before dip-coating, the fiber is first cleaned with de-ionized water and then with isopropyl alcohol. The dip-coating was done at a withdrawal rate of 7.5 cm/min. The fiber was then left to dry in air for 10 hours. After this, it was put in an oven held at 130°C for 60 minutes to dry. After drying, the fiber was sintered in air at 1000°C for 14 hours to remove any remaining organic material from the sol-gel precursor. This entire process was repeated for each layer. Multiple dip-coating cycles were performed to increase the thickness of the sol-gel derived layer. To maintain a consistency between the layers, the same batch of sol-gel was used for all the dip-coating cycles and the withdrawal rate for the dip-coating process was kept the same. One, two, three and four cycles of dip-coating were applied on three different but contiguous sections of the YAG fiber, with each section covering roughly 1 cm. The increase in thickness of the sol-gel layer due to each cycle of dip-coating was approximately 0.25 µm

The amount of holmium in each fiber section was characterized by both optical and quantitative x-ray techniques. The concentration of Ho^{3+} ions was determined by optical measurements as shown in Fig 12. Ho:YAG absorbs at 532 nm. The power absorbed increases with the increase of concentration of Ho^{3+} ions in YAG. Attenuation losses for SC Ho:YAG fibers have been measured for known Ho dopant concentrations (0.5, 1, 4%) and a general trend has been shown. By performing optical absorption measurements on the fiber sections grown from the preform with different number of HoAG layers and comparing it with the pre-established trend, an estimate of the unknown atomic percent of Ho in the different fiber sections can be obtained. Experimental measurements demonstrate that for every layer of HoAG on the source preform of 330 µm diameter increases the Ho concentration of the regrown 120 µm diameter fiber by 0.21%. Hence for example, the section grown from the preform having 2 layers of HoAG is expected to have 0.42% Ho:YAG. It is to be noted here that the SC fiber grown from the section of the preform having 1 layer of sol-gel derived HoAG has been removed. This segment had a significant “hotspot“ in the fiber which rendered its optical quality significantly poorer than the other fiber sections.

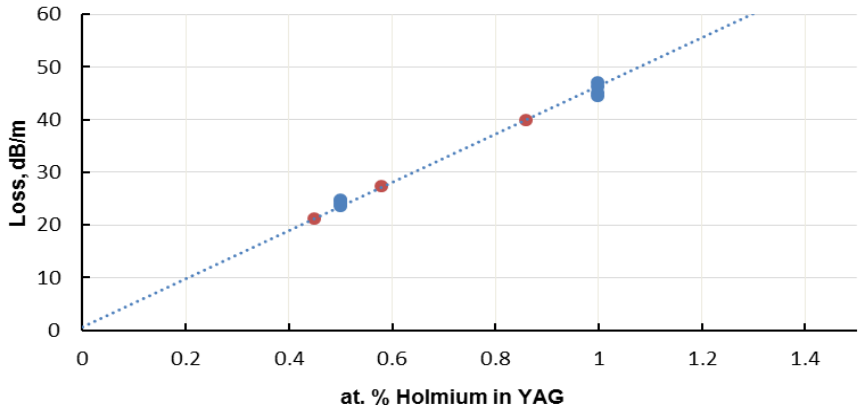

Figure 12 - Estimating concentration of Ho-ion dopant in YAG SC fiber in sol-gel coated regrown fibers, by fitting it to previously obtained absorption loss for a known concentration of holmium, shown as blue dots. The data points in orange are losses measured for SC fibers grown from preforms with 2, 3, and 4 layers of sol-gel HoAG.

The lasing characteristics of the holmium doped YAG SC fibers are studied using a modulated pump laser (10 Hz, 50% duty cycle) to reduce thermal load. Previous experiments have shown that when pumped with a 1908 nm Tm:fiber laser, Ho doped YAG SC fibers lased at 2.09 μm[13]. The lengths of the fibers grown from the preforms with 2, 3 and 4 layers of HoAG were 11 cm, 12 cm and 11 cm, respectively. The performance of the three different fibers are shown in Fig. 13. For these samples, it can be seen that the slope efficiency increased with the increase in holmium concentration of the fiber. For the fibers grown from performs having 2 and 3 layers of HoAG, the residual pump was too high suggesting that, at these fiber lengths, the Ho^{3+} ion concentration was too low for effective absorption at the pump wavelength. The slope efficiency does not show any thermally induced roll-off up to 27W of pulsed input power. This result demonstrates the good passive cooling due to increased surface-to-volume ratio for the small diameter fibers.

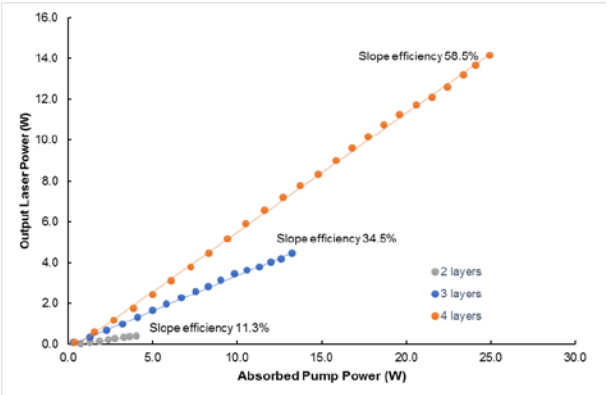

Figure 13 - Slope efficiency of Ho:YAG fibers grown from a preform with a different number of HoAG layers.

Related publications

1. "Single crystal Er3+:YAG fibers with tailored refractive index profiles," L. Cheng, T. Chick, J. Chapman, E. F. C. Dreyer, C. D. Nie, S. Bera, J. A. Harrington, and S. C. Rand, 57, pp. 362-370 (2018) doi.org/10.1364/AO.57.000362.
2. "Optimizing alignment and growth of low-loss YAG single crystal fibers using laser heated pedestal growth technique," Subhabrata Bera, Craig D. Nie, Michael G. Soskind, and James A. Harrington, **56**, 9649-9655, (2017) doi: 10.1364/AO.56.009649. http://dx.doi.org/10.1364/OE.24.015522
3. "Growth of single-crystal YAG fiber optics," Craig D. Nie, Subhabrata Bera, James A. Harrington, Optics Express, 24, 15522-15527, (2016) http://dx.doi.org/10.1364/OE.24.015522.
4. "Lasing characteristics of Ho:YAG single crystal fiber," Yuan Li, Keith Miller, Eric G. Johnson, Craig D. Nie, Subhabrata Bera, James A. Harrington, and Ramesh Shori, Optics Express, **24**, 9751-9756, (2016) doi: 10.1364/OE.24.009751.
5. "Cladding single crystal YAG fibers grown by laser heated pedestal growth," Subhabrata Bera, Craig D. Nie, James A. Harrington, Theresa Chick, Ayan Chakrabarty, Stephen Trembath-Reichert, James Chapman, Stephen C. Rand, Proc. SPIE, **9726**, pp. 97260C-1 – 97260C-9 (2016).
6. "Erbium distribution in single crystal YAG fibers grown by laser-heated pedestal growth technique," Craig D. Nie; Subhabrata Bera; Jeffrey E. Melzer; James A. Harrington; Elizabeth F. C. Dreyer; Stephen C. Rand; Stephen Trembath-Reichert; Christopher D. Hoef, Proc. SPIE **9342**, Solid State Lasers XXIV: Technology and Devices, 934204 (20 February 2015); DOI: 10.1117/12.2083588
7. "Investigation of the amplification properties of Ho:YAG single crystal fiber," Yuan Li; Zeyu Zhang; Ian Buckley; Jerome K. Miller; Eric G. Johnson; Craig D. Nie; James A. Harrington; Ramesh K. Shori, Proc. SPIE 9342, Solid State Lasers XXIV: Technology and Devices, 934205 (20 February 2015); DOI: 10.1117/12.2086858.
8. "Ho:YAG single crystal fiber: fabrication and optical characterization," Yuan Li, Eric G. Johnson, Craig D. Nie, James A. Harrington, and Ramesh Shori, Optics Express, **22**, pp. 14896-14903, 2014.
9. "Single-crystal, rare-earth doped YAG fiber lasers grown by the laser-heated pedestal growth technique," James A. Harrington, Craig D. Nie, Yuan Li, Eric G. Johnson, Elizabeth F. Cloos, Stephen C. Rand, Pedro Machado, and Ramesh K. Shori, Proc. SPIE, **8961**, Fiber Lasers XI: Technology, Systems, and Applications, 896126 (7 March 2014); DOI: 10.1117/12.2041769

Technical Staff and graduate students:

1. Prof. James A. Harrington
2. Craig Nie, graduated with Ph.D. January, 2017
3. Subha Bera, graduated with Ph.D. March, 2018

4. Single Crystal Er^{3+}:YAG Fibers with Tailored Refractive Index Profiles – University of Michigan

A. Highlights from UM research:

A major challenge in this program from the outset was finding methods to apply a cladding to crystalline fibers in essentially the same manner as glass fibers. In glass, the refractive index of the cladding may be lowered to ensure guided wave propagation through total internal reflection. Unfortunately, whereas glass can be heated to flow like a liquid while preserving the waveguiding properties, crystals do not have a glass forming region and cannot be drawn into fibers directly at all. Hence the focus of this research effort was to discover a method for cladding crystalline fibers to ensure waveguiding, and research at the University of Michigan was to characterize their dopant distributions for laser applications.

The main growth effort on this project at Rutgers was successful in preparing single crystal fibers with an effective cladding from rod-in-tube (RIT) preforms using an existing laser-heated pedestal growth (LHPG) apparatus. The preforms for these runs were assembled to furnish an high index inner core and a low index outer cladding of crystalline material. By simply varying growth speed, the LHPG approach produced fiber samples that the UM team was able to show consisted overall of single crystal fibers with graded dopant profiles. A modified strategy was proposed by the University of Michigan team to use inhomogeneous ceramic preforms, fashioned from densified nanopowder solid rods that converted to YAG upon heating as well. Straightness of 10 cm preforms was difficult to achieve with the ceramics however, even when extrusion was tried, and required a follow-on step of sintering (Figure 14). So this approach was ultimately not successful. Still, the ceramic research served to focus our effort on RIT fibers, from among the ideas put forward in our proposal.

Figure 14 - Cylindrical tube of a ceramic YAG green body, as extruded.

COMSOL simulations at Michigan were used to predict the shape of dopant concentration distributions that could be controlled by varying the LHPG growth speed as in Fig. 15. To do this, arbitrary values for the inter-diffusion coefficient had to be used initially, highlighting the need for an actual determination of D to assist future experimental designs. As described in the section on technical results, the diffusion constant was eventually determined for the first time, opening the door to realistic LHPG simulations with no free parameters.

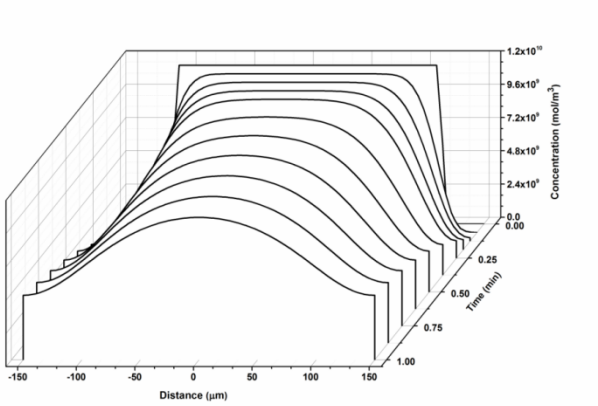

Figure 15 - COMSOL simulation of diffusion that omits conduction or surface tension effects. As time evolves, the dopant concentration decreases and the distribution broadens monotonically. The model is a 2-parameter fit based on the value of the diffusion coefficient and the dopant profile of the preform.

An alternative to RIT fiber preparation was suggested at proposal stage to investigate the use of electric fields to control dopant migration during LHPG runs. Simulations of the electric field patterns and strengths suggested that radial migration could be achieved by applying a static voltage of 1000V to a pair of ring electrodes through which the LHPG melt was intended to pass (see Figure 16). Although ring electrodes were designed and fabricated, this approach was ultimately rejected because the specifications for centering the growing fiber within the electrode were too stringent in fibers with radii of only 150 microns and could not be realized experimentally.

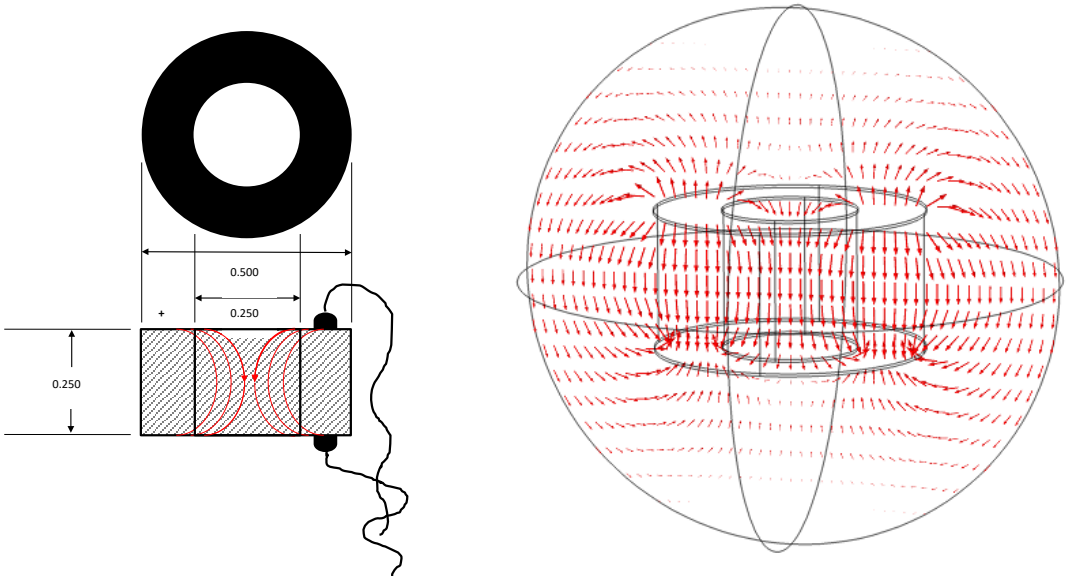

(a) (b)

Figure 16 - (a) Ring electrode design for controlled dopant migration in LHPG YAG fibers. (b) COMSOL map of the electric field distribution achievable with the ring electrode structure.

Because COMSOL simulations of diffusion (Fig. 15) indicated that program objectives could be met with RIT samples, the main focus of research at Michigan was directed to determining refractive index and dopant concentration profiles in rod-in-tube fibers as early as Year 2. Experiments on these topics required the development of polishing methods adapted for single crystal fibers. These followed attempts to cleave SC fibers which were unsuccessful, and the realization that the techniques and commercial equipment standardly used for preparing the ends of glass fibers were ineffective. Mounting and polishing of hard garnet crystalline fibers required custom procedures and unusual materials to keep the tips from "chattering" and splintering during the polishing procedure. Eventually a suitable combination of jig and materials was found that yielded good optical polishes, but flatness better than $\Delta z \sim 1$ micron at the edges of YAG end surfaces unfortunately proved to be unachievable. This had important implications for the characterization effort because small non-uniformities over the surfaces of polished fibers proved to be the chief limitation in reflective index profiling, preventing surface maps of the index (by any reflection method) at the level observed even in 50%Er-doped RIT fibers, namely $\Delta n < 0.001$. Consequently quantitative evaluation of refractive index profiles was not possible. However a highly effective method of mapping dopant gradations with the use of laser-induced fluorescence (LIF) was successfully developed with spatial resolution of a few microns. The use of laser-induced fluorescence to furnish dopant concentration maps avoided the requirement for surface flatness, provided high spatial resolution, was linear in dopant density, and sensitive. Finally, the inter-diffusion coefficient D for Er and Y in molten YAG was determined for the first time, using LIF scans of RIT fibers grown at different speeds.

B. Technical/Scientific Achievements (Yrs 1-5):

(i) Dopant Concentration Mapping by Laser-induced Fluorescence

To map the concentration of dopant ions over the cross-sections of finished fibers, a high resolution profiler was set up to image laser-induced fluorescence (Figure 17(a)). Thin slices of SC fibers were prepared from as-grown fibers by encasing them in epoxy and sectioning them into one-inch diameter disks using a diamond saw. Each disk was polished to a thickness of approximately 0.5 mm and placed in the imager where it was excited with laser radiation (λ_{ex}=532 or 514.5 nm) to generate luminescence from erbium ions. Fluorescence from the fiber sample was relayed to a spatial filter using a 2f-2f lens system to reject incident laser light and magnified 10X before being passed through a sharp edge filter to discriminate further against scattered light at the laser wavelength. Finally, the image was captured with a CCD detector.

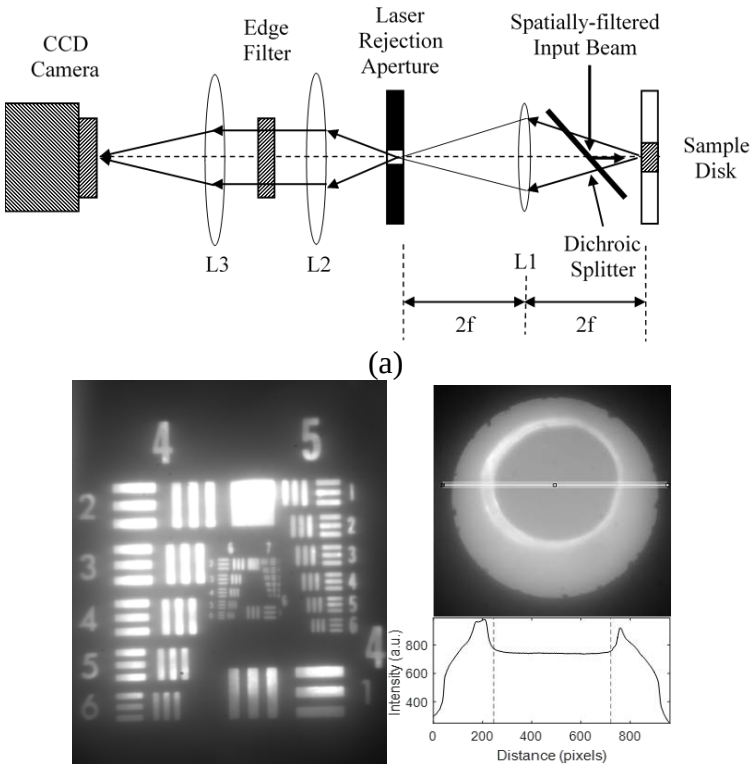

Figure 17 (a) Schematic of the fluorescence intensity mapping apparatus. Light collected by lens L1 is spatially filtered, collimated, and transmitted through an edge filter to remove light at the laser wavelength. Lenses L1, L2, and L3 are diffraction-limited achromats selected for a magnification of 10X. (b) Resolution target recorded in fluorescent light. The smallest resolvable line images are separated by 3-4 microns. (c) Flat reference distribution in a homogeneously-doped 0.5% Er^{3+}:YAG fiber. The upper portion of the figure is a cross-sectional image of the fiber taken through an opaque, circular stop. The lower portion is a lineout of image intensity along a diameter, with the fiber occupying the region between vertical dashed lines.

By replacing the sample with a resolution target, it was possible to measure the imaging performance of the apparatus directly. Figure 17(b) demonstrates lateral resolution of ~3.5 microns. Relative intensity variations of the incident light distribution were verified to be much less than 1% across the sample region by imaging an SC fiber grown from a homogeneous preform of 0.5% Er^{3+}:YAG in its own fluorescence (see Figure 17(c)). This ensured that variations observed in RIT fibers were due to real concentration gradients rather than non-uniformities of the input field distribution.

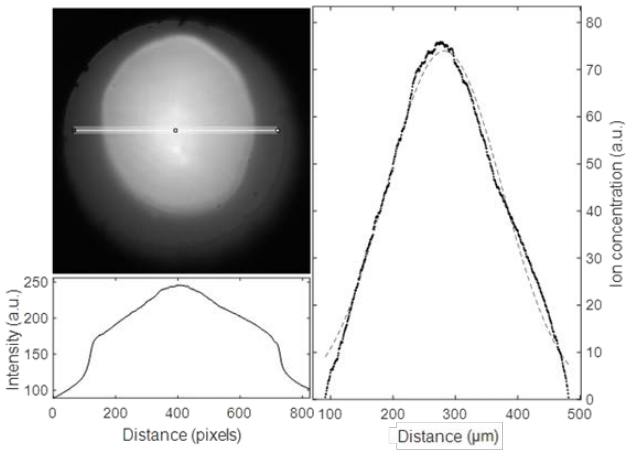

(a)

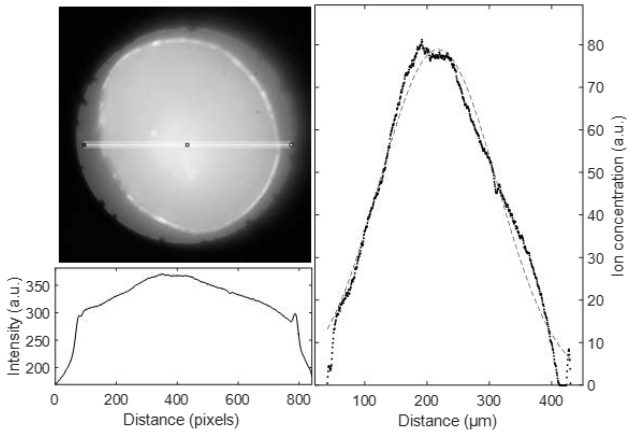

(b)

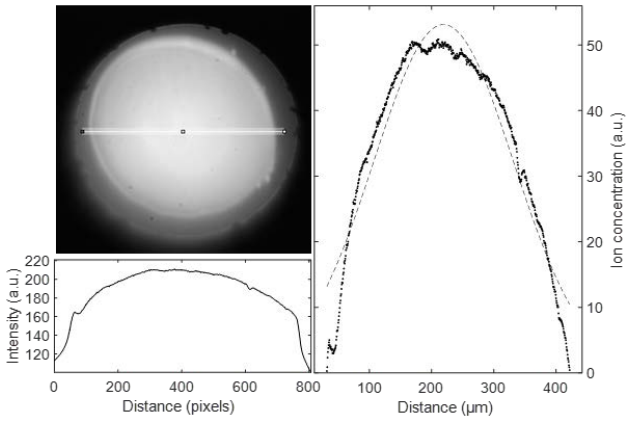

(c)

Figure 18 - Er^{3+} distribution in 50% Er^{3+}:YAG core with pure YAG cladding grown at (a) 3, (b) 2, and (c) 1 mm/min. The profiles are one-dimensional lineouts through fluorescent images giving dopant concentration versus position across each fiber sample. Gaussian fits to the experimental reflectivity profiles within each fiber are shown on the right.

Dopant concentration profiles of rod-in-tube fibers grown from 50% Er^{3+}:YAG cores were recorded using the approach outlined above. Due to selective excitation of Erbium ions by the incident laser, and the strict proportionality of re-emission intensity to excited state density, the brightness in fluorescence images provided a spatial map of the distribution of Erbium ions that was linear in dopant concentration. Significant differences were noted for fluorescent profiles of fibers grown at different speeds. In all RIT samples free of internal cracks, the brightness of fluorescence images exhibited a peak near the center of the fiber cross section. Simulated and experimentally-measured concentration profiles acquired for 50% Er^{3+}:YAG fibers grown at speeds of 1, 2 and 3 mm/min are presented in Figure 19.

In experimental profiles (Fig. 19(c) the position of the Er concentration peak was not always centered. Offsets originated from random asymmetries of the preforms and the mere fact that the fibers themselves were not circular in cross section. Post-growth distributions of erbium ions revealed that as the time in the melt increased the width of the ion profile, consistent with the idea that thermal diffusion should take place from the high concentration of ions in the preform core toward the periphery. A quantitative comparison of fluorescence profiles in these samples was therefore undertaken to determine the inter-ion diffusion coefficient which determines dopant migration.

(ii) Observation & Analysis of Diffusion Dynamics in LHPG SC-fibers

The evolution of the ion distribution in RIT samples was simulated as a function of melt time (inverse growth speed) based on a 2-parameter model (see Cheng et al.). The results are shown in Fig. 19. Clearly as time goes on the initial concentration of Er^{3+} impurities diffuses away from the center of the fiber. Figure 19(b) summarizes the dependence of the width of ion distributions on melt time that is expected over the timescale of our experiments. The dashed curve indicates that a few seconds are required for the initial rectangular distribution to evolve into a Gaussian shape, but once it becomes Gaussian this shape is maintained and the square of the distribution width (σ^2) grows steadily with time until the outer boundary of the fiber is reached, preventing further outward diffusion. At this point a uniform background begins to accumulate and a straight line prediction begins to underestimate the width of the distribution. The concentration profile rapidly flattens, becoming increasingly non-Gaussian. For this reason, at long times the distribution of ions in the fiber progressively deviates from that predicted for diffusion in an infinite medium with no boundaries.

Cheng et al. also used an analytic expression for the width of a Gaussian-shaped concentration gradient undergoing diffusion for a time t in an infinite medium to fit the experimentally measured ion distributions shown in Figure 19(c).

$$\sigma^2(t) - \sigma^2(0) = 2Dt$$

Estimates of the diffusion coefficient based on the analytic expression above and the COMSOL simulations agreed well. Hence it was possible to report an experimental value for the diffusion coefficient of inter-diffusion of Er^{3+} and Y^{3+} in YAG at T=2000 ^{o}C for the first time. The reported value was $D=(9.10+/-0.8)x10^{-11}$ m^2/s.

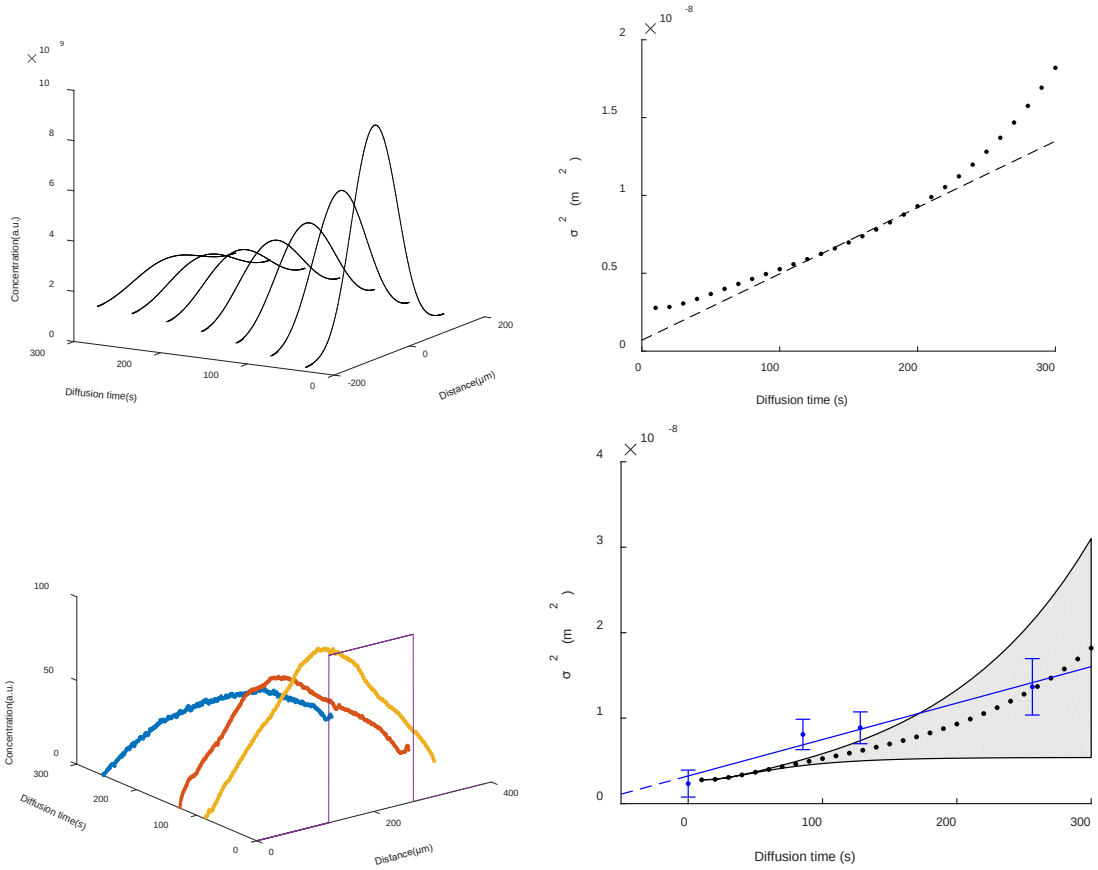

Figure 19 - (a) Ion distributions versus time in the melt (the “diffusion time”), simulated by the COMSOL thermal diffusion model. (b) Simulation widths of ion distributions (dotted), together with a straight line for comparison. (c) Measured ion distributions versus diffusion time (time in the melt calculated from inverse growth rate). (d) Best analytic fit to the data of Fig. 19(c), for fibers grown at 1,2 and 3 mm/min.

In summary, Er^{3+}:YAG fibers grown from RIT preforms by the LHPG technique at speeds in the range of 1-3 millimeters per minute yielded single-phase, single-domain crystals with graded dopant distributions. The distributions, determined with high resolution laser-induced fluorescence imagery exhibited a systematic trend, developing progressively wider distributions versus time-in-the-melt at constant laser power. Results for post-growth Er^{3+} ion distributions were well-described by a numerical model based on Fick’s equation with a single value of diffusion constant. Determination of the D value opens the door to more precise LHPG experiments in the future.

C. People supported & Destinations

(i) Graduate Students

Theresa Chick – 50%, 50%

Michael Purcell – 50%, 50%

Long Cheng – 50%, 50%

Nate Taylor – 0%,0%

(ii) Faculty
Stephen Rand – 5%, 5%
Richard Laine – 0%,0%

(iii) Undergraduate Students
Logan Stagg – 0%, 0%
Stephen Trembath-Reichert – 5%, 0%
Christopher Hoef – 5%, 0%
James Chapman – 5%,0%

(iv) Graduating Undergraduate Metrics:
Number who graduated during this period - 4
Number who graduated during this period with a degree in science, mathematics, engineering, or technology fields - 4
Number who graduated during this period and will continue to pursue a graduate or Ph.D. degree in science, mathematics, engineering, or technology fields - 4
(Christopher Hoef, Logan Stagg, Anderson C. Mendes, James Chapman)
Number who achieved a 3.5 GPA to 4.0 (4.0 max scale) - 4
(Christopher Hoef, Logan Stagg, Anderson C. Mendes, James Chapman)

(v) Number funded by a DoD funded Center of Excellence grant for Education, Research and Engineering - 0

(vi) Number who intend to work for the Department of Defense - 1

(vii) Number who will receive scholarships or fellowships for further studies in science, mathematics, engineering or technology fields - unknown

(viii) Degrees Awarded
Master's - 1 (Theresa Chick)
Ph.D. – 1 (E.F.C. Dreyer)

D. Honors & Awards

S.C. Rand, Distinguished Speaker, Indian Institute of Technology Kharagpur (2014)
S.C. Rand, Erskine Fellow, University of Canterbury NZ (2014)
S.C. Rand, APS-IUSSTF-Professorship (2013)
S.C. Rand, OSA Travel Fellowship (2013)
E.F.C. Dreyer, NSF Fellowship (2013-2018)
A. C. Mendes, CNPQ Brazilian Study Abroad Scholarship (2016)

E. Publications

(a) Journal articles

L. Cheng, T. Chick, J. Chapman, E. F. C. Dreyer, C. D. Nie, S. Bera, J. A. Harrington, and S. C. Rand, "Single Crystal Er3+:YAG Fibers with Tailored Refractive Index Profiles, Applied Optics 57. 362(2018).

(b) Peer-reviewed Conference papers

J.A. Harrington, C.D. Nie, E. Cloos, S.C. Rand, Y. Li, and E. Johnson, "Single-crystal, rare-earth-doped YAG fibers grown by the Laser Heated Pedestal Growth Technique", Annual Meeting of the Optical Society of America (FiO'13), Orlando, Florida, FTu4B.4.

E. F. Cloos, L. Stagg, S. Trembath-Reichert, C. D. Nie, J. A. Harrington, and S. C. Rand "Single-crystal Er:YAG Fiber with graded dopant concentration for high power lasers", International Conference on Luminescence, Wroclaw, Poland, July 13-18 (2014).

Craig D. Nie, Subhabrata Bera, James A. Harrington, Nathan Taylor, Richard M. Laine, Elizabeth F. C. Dreyer, Stephen C. Rand, S. Trembath-Reichert, Rare-earth doped, single-crystal fibers grown from ceramic and single crystal preforms, Photonics West, San Francisco, Feb. 8-13(2015), paper [9342-3].

E. F. C. Dreyer, L. Stagg, S. Trembath-Reichert, C. Hoef, C. D. Nie, J. A. Harrington, and S.C. Rand, "Fabrication and Characterization of Fiber Waveguides from Single-Crystal Er3+- Doped YAG", Conference on Lasers and Electro-optics (CLEO '15), San Jose, California, May 10-15, 2015, paper JTh2A.

Craig D. Nie, Subhabrata Bera, James A. Harrington, Nathan Taylor, Richard M. Laine, Elizabeth F. C. Dreyer, Stephen C. Rand, S. Trembath-Reichert, Rare-earth doped, single-crystal fibers grown from ceramic and single crystal preforms, Photonics West, San Francisco, Feb. 8-13(2016).

5. Ho:YAG SCF Amplifier Work – Clemson University

0.5% Holmium (Ho) doped YAG single crystal fiber (SCF) was fabricated using Laser Heated Pedestal Growth (LHPG) method and characterized for its optical absorption and emission properties involving transitions between the $^5I_8$ and $^5I_7$ energy levels. The results verified the absorption peaks suitable for in-band direct pumping at 1908 nm and 1932 nm with the emission occurring between 2050-2150 nm. Small signal gain measurements were also performed for demonstrating the fiber like characteristics of the SCF.

The $^5I_8 \rightarrow {}^5I_7$ absorption spectrum of the 0.5% Ho:YAG SCF sample was measured by a mid-infrared IPG tunable laser (Model HPTLM-Cr-ZnS/Se) using a resolution of 0.7 nm. The absorption spectrum shows the strongest absorption peak is at 1907.7 nm with a full width at half maximum (FWHM) of ~ 6 nm. Note that across the spectral region accessible with the tunable laser, the absorption spectrum has an average low loss of 0.02 cm^{-1}. The measured absorption spectrum is normalized and then used to calculate the absorption cross section of the Ho:YAG SCF and confirm the peak emission in Ho:YAG SCF at 2090 nm, see Fig. 20.

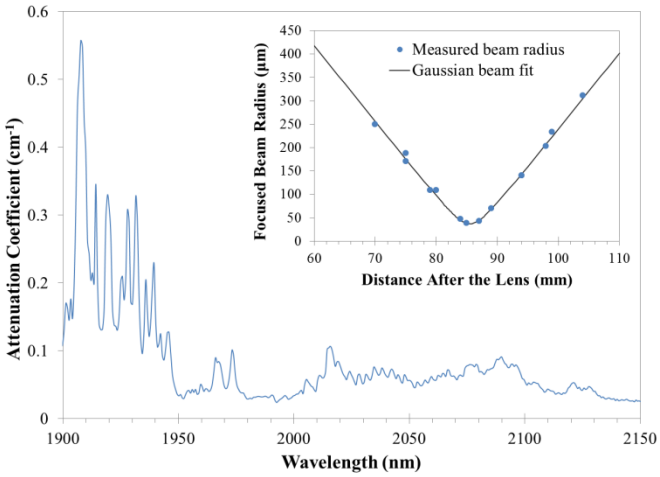

Figure 20. - The absorption spectrum of the Ho:YAG SCF. (Inset) The measured incident laser beam size with respect to the distance from the focusing lens.

To verify the calculated emission cross section spectrum, the actual fluorescence emission spectrum from $^5I_7 \rightarrow {}^5I_8$ was recorded using the IPG tunable laser for in-band pumping; and the measured fluorescence shows an emission peak is at 2090.6 nm, which is close to the calculated emission peak of 2090 nm, see Fig. 21.

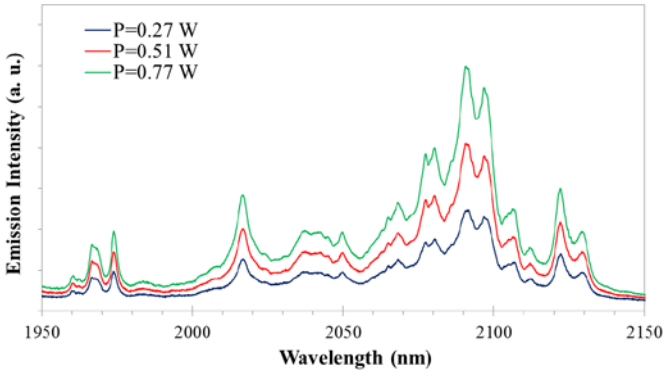

Figure 21 - The measured emission spectrum under different pump power using 1932.2 nm direct in-band pumping.

Small signal gain is also measured and simulated by a simplified quasi-four-level rate equation based fiber amplifier model, plotted in Fig. 22. These results are strongly encouraging for using Ho:YAG SCF as waveguiding gain media for laser amplification and laser generation.

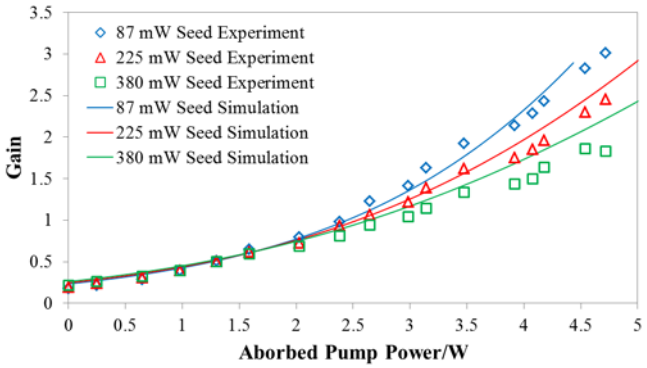

Figure 22 - Small signal gain with increasing pump power for three different seed power. Empty markers are experiment data while colored lines are simulation curves.

Ho:YAG SCF simulation

So far, due to the limitation of fabrication techniques, current SCFs are still highly multi-mode waveguides. Most of the current work on SCF amplifiers are still treating the SCF as bulk material. Theoretically, the large simulation area (large SCF cross section diameter) and complicated mode behavior during propagation increase the simulation difficulties. In our work, a numerical method based on finite difference (FD) beam propagation method (BPM) combined with the rate equations was developed for theoretical simulation. The results are encouraging to demonstrate the advantages of SCF for its fiber-like beam guiding property and solid state material gain property. The simulation tool provides details about how the fiber shape and launched mode affect the gain and output beam shape as well as predicting the amplification behavior of such unique specialty fibers.

Since SCF is a highly multimode waveguide, how the beam propagates in the SCF will depend on the incident beam shape, launching condition, and SCF geometry. Thus, a 3-D beam propagation model will be needed to predict the output mode. The pump and signal beams will have different intensity distributions at the same cross section all along the SCF, which means the pump and signal beam overlap will be different along the SCF. Models based on consistent pump and signal beam overlap, either for fiber amplifier or bulk amplifier, are not suitable for these scenarios. The performance of Ho:YAG SCF as a gain waveguide is studied and a 3-D BPM model with gain block incorporated is used for simulation. Due to the geometry imperfections of the SCF, maintaining the mode quality while propagating along the SCF is difficult. However, the simulation shows the feasibility of guiding the input beam and predicting the output beam. With proper launching conditions, matching the mode size of the SCF, and maturing the fabrication method, it is possible to maintain the input beam shape with minimum degradation at the output end of the SCF.

$$j2kn_0\frac{\partial\phi_x}{\partial z}=\frac{\partial}{\partial x}\left[\frac{1}{n^2}\frac{\partial(n^2\phi_x)}{\partial x}\right]+\frac{\partial^2\phi_x}{\partial y^2}+(k^2n^2-k^2n_o^2)\phi_x \quad (1)$$

$$j2kn_0\frac{\partial\phi_y}{\partial z}=\frac{\partial}{\partial y}\left[\frac{1}{n^2}\frac{\partial(n^2\phi_y)}{\partial y}\right]+\frac{\partial^2\phi_y}{\partial x^2}+(k^2n^2-k^2n_o^2)\phi_y \quad (2)$$

One-way paraxial semi-vector wave equations shown in Eqs. (1) and (2) are used to simulate the propagation of the field inside the SCF and can be solved numerically by an FD approximation at a small distance Δz, by iterating the process that the beam propagates in the +z direction until the desired length is reached.

$$\frac{N_{2(m,k)}(z)}{N_{1(m,k)}(z)} = \frac{\dfrac{[P_p^+(z)+P_p^-(z)]\sigma_{ap}\Gamma_{p(m,k)}}{h\nu_p A_{(m,k)}} + \dfrac{P_s^+(z)\sigma_{as}\Gamma_{s(m,k)}}{h\nu_s A_{(m,k)}}}{\dfrac{[P_p^+(z)+P_p^-(z)]\sigma_{ep}\Gamma_{p(m,k)}}{h\nu_p A_{(m,k)}} + \dfrac{1}{\tau} + \dfrac{P_s^+(z)\sigma_{es}\Gamma_{s(m,k)}}{h\nu_s A_{(m,k)}}} \quad (3)$$

$$\frac{dP_s^+(z)}{dz} = \sum_m \sum_k \left[\sigma_{es} N_{2(m,k)}(z) - \sigma_{as} N_{1(m,k)}(z)\right]\Gamma_{s(m,k)} P_s^+(z) - \alpha_s P_s^+(z) \quad (4)$$

$$\pm\frac{dP_p^\pm(z)}{dz} = \sum_m \sum_k \left[\sigma_{ep} N_{2(m,k)}(z) - \sigma_{ap} N_{1(m,k)}(z)\right]\Gamma_{p(m,k)} P_p^\pm(z) - \alpha_p P_p^\pm(z) \quad (5)$$

$$A_{(m,k)} = \Delta x \cdot \Delta y \quad (6)$$

$$\Gamma = \frac{\psi(m\Delta x, k\Delta y)}{\sum_m \sum_k \psi(m\Delta x, k\Delta y)} \quad (7)$$

The TR steady-state rate equations shown in equation (3)-(7) are used for calculating the pump and signal power change. These equations are assuming a most general two-level energy system including saturation absorption and saturation emission, which works for either a four-level or a three-level transition that may or may not include excited state absorption. Combine the above mentioned two sets of equations and iterate over small steps, the output signal E field distribution and power change can be obtained for given input conditions.

The actual SCF cross section shows some asymmetry in geometry, which yields mode mixing and mode quality degradation along the beam propagation. Fig. 23(a) shows the actual SCF geometry of 240 μm in diameter . Fig. 23(b) and (c) show the simulated output beam intensity of input Gaussian beams with $1/e^2$ width of 77 μm and 10 μm, respectively.

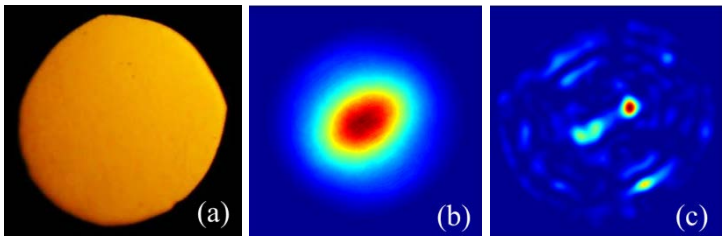

Figure 23 (a) The microscope image of the SCF cross section (polished end facet). (b) The simulated output beam intensity distribution of a 77 μm Gaussian input beam using the actual fiber shape. (c) The simulated output beam intensity distribution of a 10 μm Gaussian input beam using the actual fiber shape.

SCF Laser Work

Lasing was demonstrated at 2.09 µm in 0.5% Holmium (Ho) doped YAG single crystal fiber (SCF) fabricated using the Laser Heated Pedestal Growth (LHPG) method. The fiber diameter was 330 µm. Output power of 23.5 W with 67.5% optical-to-optical slope efficiency is, to the best of our knowledge, the highest output power achieved at 2 µm from a SCF.

The lasing cavity consisted of a flat-flat high reflector (HR) and the uncoated distal end-facet of the SCF which provides 8% Fresnel reflection as the output coupler (OC), shown in Fig. 24. The HR was placed as close as possible to the front facet of the SCF to provide as much feedback as possible for the lasing wavelength. The LHPG method fabricated Ho:YAG SCF has a diameter of 320 µm and 115 mm in length with both ends polished. The 1908 nm Tm:fiber pump laser was operated in a pulse mode with a pulse repetition frequency of 10 Hz and a duty cycle of 50% to reduce the thermal load in the crystal rod.

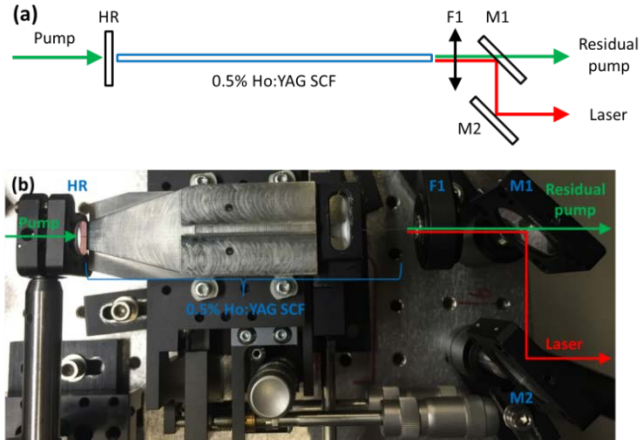

Fig. 24 - (a) Schematic of Ho:YAG SCF laser setup and (b) actual setup.

The optical-to-optical slope efficiency was measured to be 67.5% with a lasing threshold of 3.3 W; and the maximum output laser power is measured to be 23.5 W, shown in Fig. 25.

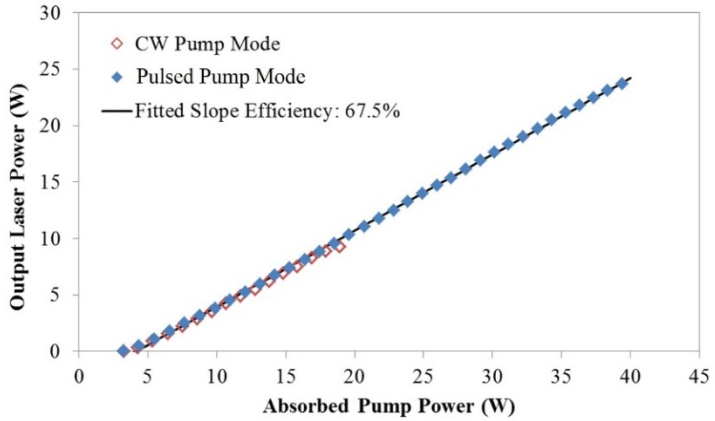

Figure 25 - The output laser power as a function of absorbed pump power under both CW and pulsed pump mode.

The spectrum of the output laser beam at the output power of 22 W is shown in Fig. 26 on a linear scale. The laser wavelength is centered at 2090.6 nm with a full width at half maximum (FWHM) of 1.3 nm. Given the large diameter of the SCF and absence of any intra-cavity spatial mode control, the output laser beam is highly multimode.

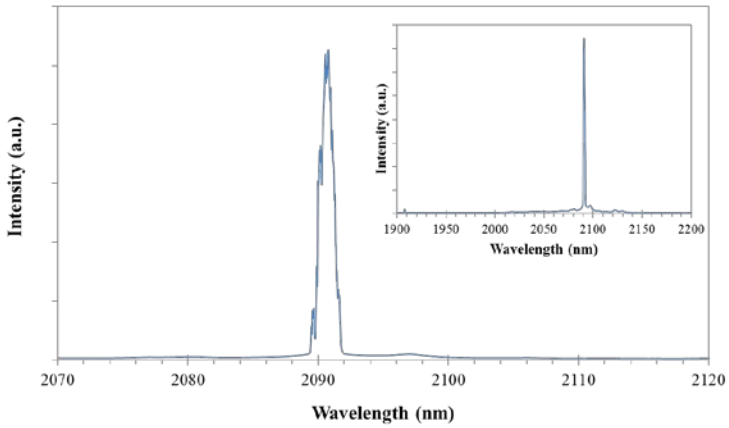

Figure 26 - The optical spectrum of the laser at 20 W of output power centered at 2090.6 nm. The inset shows the whole spectrum from 1900 – 2200 nm.

With efforts in reducing the diameter of SCF and scattering loss, better diameter variation control, cladding, better modal control, and more efficient thermal management, significant improvement in the power scaling as well as the spatial beam quality of laser output beam from SCF will be achieved in the near future. Significant improvements in the fabrication of the air clad 0.5% Ho:YAG SCF using LHPG technique have led to a demonstration of the highest output power at 2090.6 nm reported to date. This SCF has multiple bounces of the pump and signal beam, thus making it a true optical waveguide. The maximum output laser power of 23.5 W was achieved with optical-to-optical slope efficiency of 67.5%. A reduction in the diameter of SCF, better diameter variation control along the length of the SCF, cladding, and better thermal management will lead to significant improvement in the power scaling as well as the spatial beam quality of laser output beam from SCF. These results can also be extended further based on improvements in the cladding interface and result in viable solutions for a number of high power laser applications.

Ho:YAG Rod Amplifier Work

A. Single Beam Amplification

The amplification of concentric vortex beams has been demonstrated for the first time in a rod amplifier. A rod amplifier is a frontier approach in solid state systems combining the advantages of the conventional bulk crystal materials and optical fiber systems. Typically the seed goes through the rod as in free space while the pump is wave-guided by the rod. However, the design can be rather flexible depending on the applications, such as to increase the modal overlap between the seed and the pump and therefore increasing the gain performance. The rod is long enough to provide sufficient gain to the input seed beam while the integrity of the beam mode is maintained well through the rod. The small diameter of the rod helps with the confinement of the pump and it is potentially possible for the rod to work as a power amplifier.

Figure 27 - (a) shows the single-pass, co-pumping amplifier setup utilizing the 1% Ho:YAG rod. The ends of the 1mm diameter × 60 mm long Ho:YAG rod were polished to flat/flat finish and AR coated for both the pump and the seed wavelengths (1.9 – 2.1 μm). The barrel of the Ho:YAG rod was also polished so the rod can be used as a waveguide for the pump light if needed. A Tm:fiber laser (IPG TLR-50) was used as the pump source, which provided single mode 1908 nm laser output. The pump laser was operated in a modulated mode with a pulse repetition frequency of 10 Hz and a duty cycle of 50% to reduce the thermal load in the crystal rod. The phase plate converts the Gaussian seed beam into the desired concentric vortex beam shape, the (1+2) and (1+4) concentric vortices, corresponding to 3-lobe and 5-lobe vortices, were investigated. Illustrations of the phase wrap and the microscope images of the fabricated phase plates are shown in Figs. 27(b)-(e).

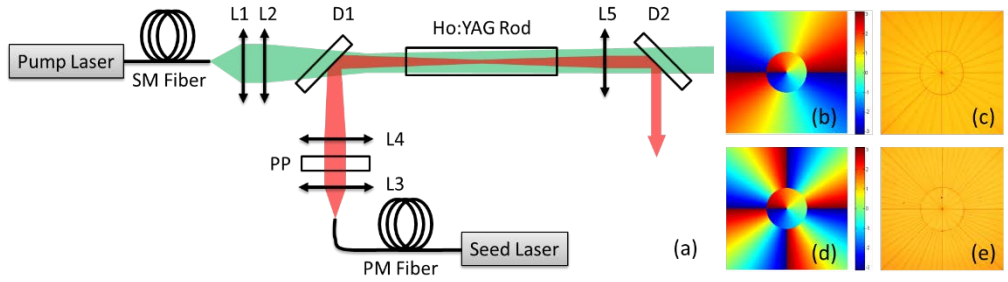

Figure 27 - (a) Experimental setup of the Ho:YAG rod amplifier. (b) The simulated phase wrap; (c) the microscope image of the fabricated phase plate for the 3-lobe concentric vortex. (d) The simulated phase wrap; (e) the microscope image of the fabricated phase plate for the 5-lobe concentric vortex.

The images of the output seed through the rod without the pump were also taken, shown in Figs. 28. These images support the premise that spatial characteristics of vortex beam are preserved while propagating through the rod.

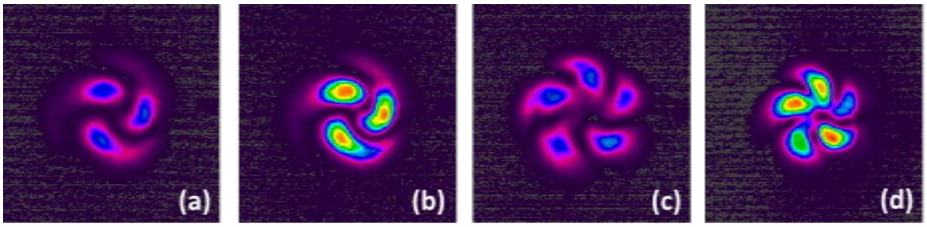

Figure 28 - The images of the concentric vortex beam through the rod amplifier; (a) and (c), with no pump; (b) and (d) with 20 W of incident pump power.

Figure 29 - (a) and (b) show the output seed power versus the incident pump power for 0.1 W incident seed power and 0.5 W incident seed power, respectively. Both the 3-lobe and the 5-lobe vortex beams were measured at each incident seed power. The output power is simulated using the above mentioned BPM model with steady-state rate equations.

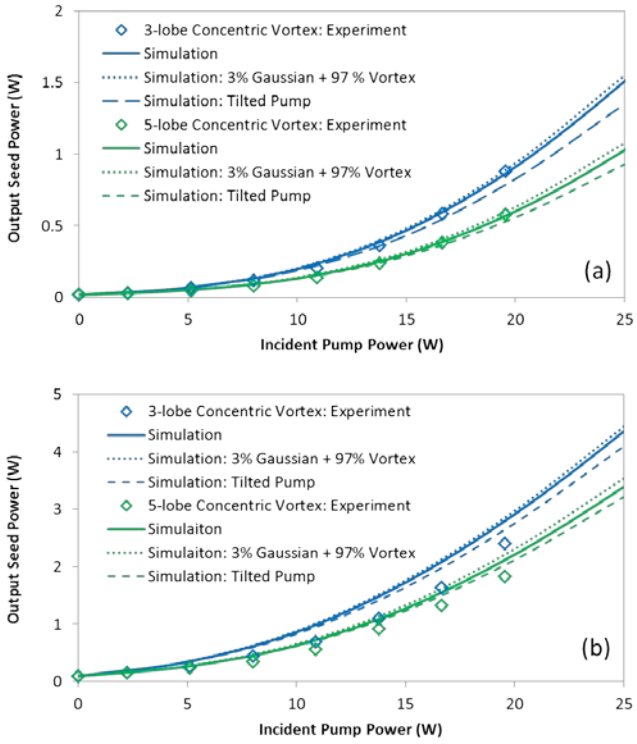

Figure 29 - The measured output seed power for different concentric vortex beams. (a) Incident seed power of 0.1 W; (b) incident seed power of 0.5 W. Blue for 3-lobe concentric vortex and green for 5-lobe concentric vortex. Solid lines, simulations of ideal cases; Dashed lines, simulations of a 0.3 degree tilted incident pump beam. Dotted line, simulations of 3% Gaussian and 97% concentric vortex.

In conclusion, we demonstrated the amplification of concentric vortex modes through a rod amplifier experimentally and theoretically.

Beam multiplexing and amplification

The multiplexing and amplification of 2 μm vortex beams are experimentally verified in a Ho:YAG crystal rod amplifier. Spatially multiplexed vortex beams are studied and the amplification results are presented and discussed. The integrity of the launched vortex beams is well maintained through the amplification process. The capability of spatially multiplexing and simultaneous amplification of the rod amplifier is shown. Benefiting from the large spatial area of the rod, the system shows potential to amplify multiple spatially multiplexed incoherent or coherent vortex beams. Further discussions are provided to increase the gain as well as for power scaling. Because of the nature of Ho:YAG material and the geometry of the rod amplifier, the system shows potential of working as a power amplifier for vortex beams.

The 1% Ho:YAG rod had a diameter of 1 mm and a length of 60 mm; both end-facets were anti-reflection (AR) coated for the pump and seed wavelengths. Two 2091 nm charge |4| vortices were multiplexed and propagated through the rod amplifier system. The phase plates to generate the vortex beams were etched in a fused silica wafer and designed with a corresponding $|l|\times 2\pi$ wrapping phase at the seed wavelength of 2091 nm, with $|l|$ being the charge number of the

generated vortex beam. A Gaussian beam passing through the phase plate will carry the spiral phase and form an intensity singularity in the center. The two vortices spatially overlap with each other and occupy the same volume inside the Ho:YAG rod. For the purpose of demultiplexing, two vortices have the opposite OAM charge, one is +4 and the other is -4, and the two vortices are on orthogonal polarization states to prevent any interference, shown in Fig. 30.

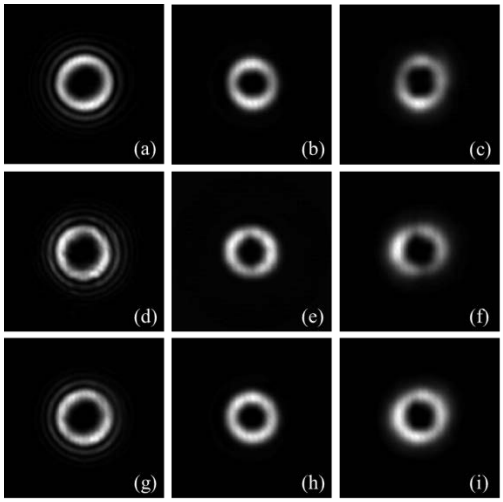

Figure 30 - The images of the charge +4 vortex beam (a) in free space; (b) through the rod; and (c) amplified. The images of the charge -4 vortex beam (d) in free space; (e) through the rod; and (f) amplified. The images of the multiplexed two vortex beams (g) in free space; (h) through the rod; and (i) amplified.

A Tm:fiber laser was used as the pump source, which provided a single mode 1908 nm laser output. The pump laser was operated in a pulse mode with a pulse repetition frequency of 10 Hz and a duty cycle of 50% to reduce the thermal load in the crystal rod. The amplification of each individual vortex and the combined multiplexed vortices were measured. The two vortices occupied almost the same spatial volume and yielded the same amplification results. Adding the amplified powers for each vortex when measured separately shows good agreement with the total output power with both vortices amplified simultaneously, shown in Fig. 31.

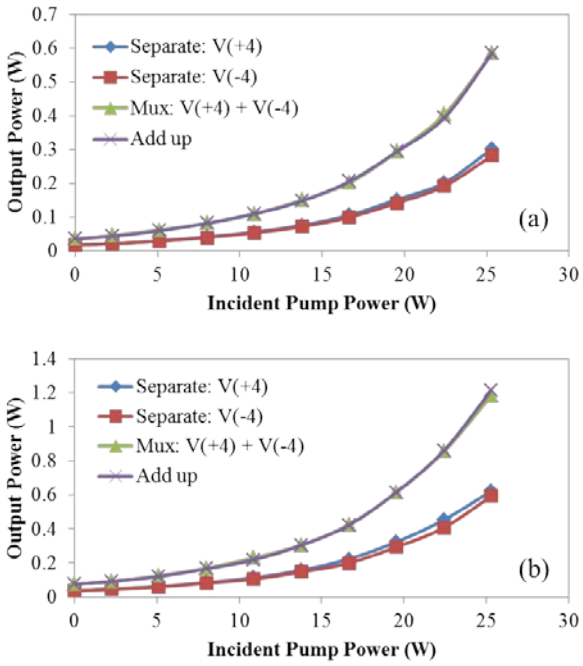

Figure 31 - The measured output seed powers of spatially multiplexed charge +4 and charge -4 vortex beam as a function of the incident pump power with both modes having incident seed power of (a) 0.1 W and (b) 0.2 W.

To study the phase integrity of the amplified vortices, a matched filter system was set up after the rod amplifier. This matched filter involves using a conjugate phase plate and looking at the correlation peak at the focal point of the system. If the conjugate phase plate matches the phase of the incoming beam, a strong correlation will appear on axis as a bright spot. If the phase of the incoming beam has changed or degraded due to the amplification process, the correlation spot will be less intense. By measuring the power in the correlation spot at different pumping levels, it is possible to study the phase preservation of the amplified vortex. The measured correlation peak stays the same at all pump levels. Since both the vortices have the same power and the same gain; this is a strong indication that the phase is preserved throughout the amplification process.

High order mode amplification in Ho:YAG SCF

A. Single mode excitation and amplification

Since the cladding technique for SCF is still under development, we had to utilize the multimode nature of the Ho:YAG SCF. We explored the selective coupling and excitation of different spatial modes, the fundamental TE_{00} mode and the higher order TE_{11} mode, individually, in the air-clad Ho:YAG SCF working as a multimode waveguide amplifier.

The 0.5% Ho:YAG SCF used for studying is 340 μm in diameter and 103 mm in length with both ends polished. A collimated 1908 nm single mode pump beam is focused down to 200 μm in diameter at the entrance facet of the SCF. The output of a tunable IPG laser (IPG HPTLM Cr:ZnS/Se, set at 2091 nm) is coupled into a single-mode (SM) 10/125 polarization-maintaining (PM) fiber; and used as the seed delivery fiber to ensure high mode quality. For the excitation of

the TE_{00} mode, the output of the PM fiber is focused down to approximately 220 μm at the entrance facet of the SCF to match the size of the TE_{00} mode of the SCF. For the excitation of the TE_{11} mode, a diffraction phase plate (DPP) for generating the matching pattern is placed between L1 and L2. The DPP has a phase profile identical to that of the TE_{11} mode and will transform the incident Gaussian beam to a pattern closely matching the intensity profile of the TE_{11} mode. The diagram and images of the set up and mode patterns are shown in Fig. 32.

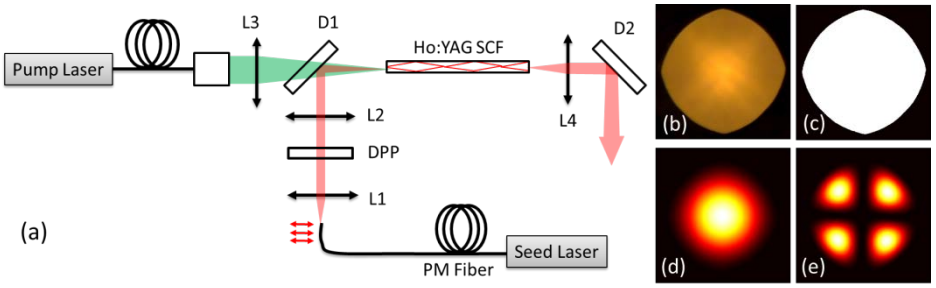

Figure 32 - (a) Experimental setup. (b) Ho:YAG SCF cross section image. (c) SCF index profile for mode solving. n=1.81. (d) Eigenmode LP_{01}. (e) Eigenmode LP_{21}.

The output seed beam from the SCF amplifier is observed in the far field, shown in Fig. 33 together with the measured output power.

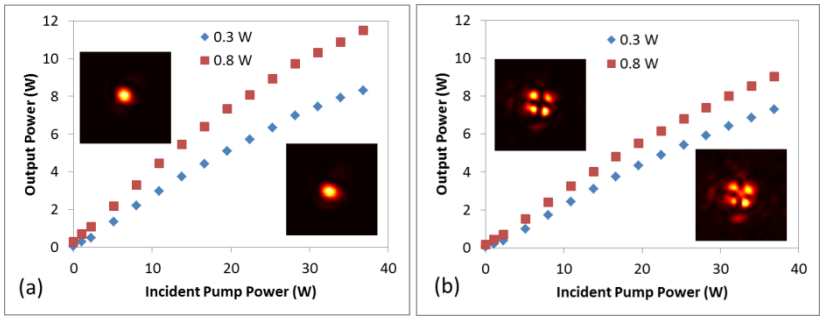

Figure 33 - Measured output power of the launched (a) LP_{01} mode; (b) LP_{21} mode.

For the launched TE_{00} mode or TE_{11} mode, the beam shape degrades with increasing pump power, which indicates that the launching conditions are not optimized and other modes in the SCF are excited. Further work will be carried out to closely match the desired spatial mode in the SCF and pumping with the corresponding spatial mode for higher gain and better beam shape preservation. Overall, the air-clad SCF shows great potential as a higher order spatial mode amplifier.

B. Coherent high order modes multiplexing and amplification

Then the selective coupling and simultaneous amplification of two higher order spatial modes, the two orthogonal HOMs of TE_{11a} and TE_{11b}, are demonstrated both in simulation and experiment. In order to achieve higher mode coupling efficiency and better mode purity, simulation of the SCF eigenmode sets are carried out for a better understanding of the targeted mode properties due to the unique square shape of the SCF cross-section. Semi-vectorial formulation is used for solving the true linearly polarized quasi-TE modes and is solved numerically using finite-difference (FD) discretization in MATLAB. By comparing the beam profiles of the simulated eigenmode and the incident beam, calculating the modal overlap, and

optimizing the incident beam size, a high modal purity of ~ 90% is predicted for the targeted TE_{11} modes.

The experimental setup is similar as before, but modified for coupling two modes simultaneously. For the pump beam, a charge 2 vortex phase plate is used to make the pump beam a ring-shaped profile with better modal overlap with the intensity summation of both TE_{11a} and TE_{11b} modes. The two horizontally polarized incident beams are split from one seed laser set at 2090 nm shown in Fig. 34. The two horizontally polarized incident beams are split from one seed laser (IPG HPTLM Cr:ZnS/Se) set at 2090 nm; and the coherence between the two beams is removed by using delivery fibers of different lengths. The SCF is fabricated by the Laser heated pedestal growth (LHPG) method using an orientated seed at a specific orientation yielding a square shaped cross section and smooth sidewalls with no crystal facets, same as used in previous section.

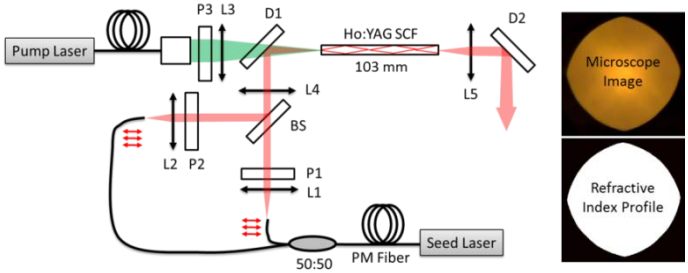

Figure 34 - Experimental setup using square-shaped SCF cross section profile (center). Inset, output image of the simultaneous amplification of modes TE_{22a} and TE_{22b} at highest output power.

When the two modes are incoherent, the combination of the two modes will just simply be the overlapped intensity profile. Using the incident seed power of 270 mW for each mode, the amplified output power is measured and shown in Fig. 35 together with the simulated output power. The simulations fit the measured results very well, except for some power roll-over, which is likely caused by the lack of proper cooling due to the quasi-three level nature of Ho:YAG material.

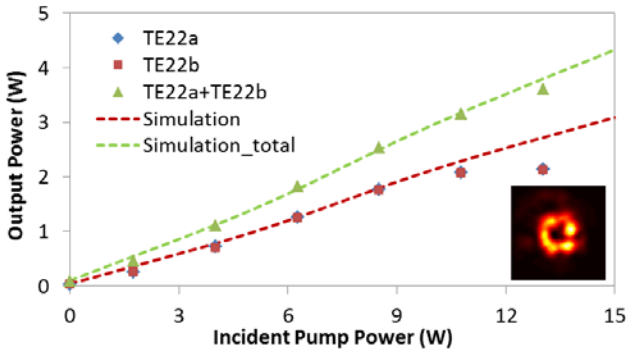

Figure 35 - The measured and simulated output power measurements of two incoherent modes.

Figures 36 (e) and (j) show the amplified individual beam output. Comparing these with the output beams shown in Fig. 36(d) and (i) without amplification, the amplified beams maintain the 4-lobe intensity profile very well.

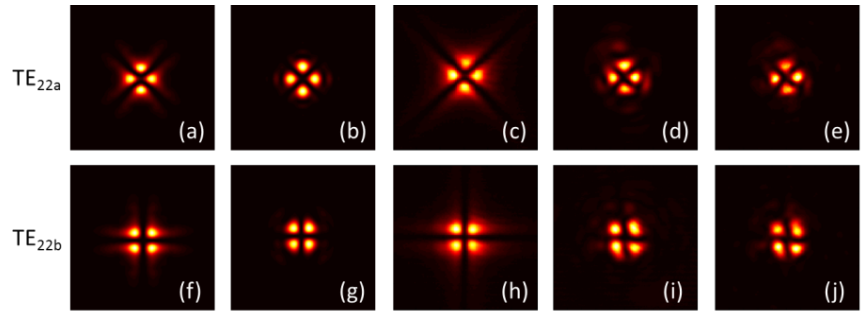

Figure 36 - The beam shape comparison between simulation and experiment. (a) and (f), simulated incident beams; (b) and (g), simulated output beams; (c) and (h), measured incident beams; (d) and (i), measured output beams without pump; (e) and (j), measured amplified beams at 11 W pump.

By matching the delivering fiber length and therefore matching the optical path length, the coherence between the two seeds is restored. Using an electro-optic phase modulator (EOM) in one of the seed beam paths, the relative phase between the two seeds can be adjusted. When this relative phase delay is 0 or π, the coherently combined seeds are TE_{22}-like patterns with the location of the lobes positioned between the individual eigenmodes. This is shown in Fig. 37 for both simulation and experimental results, with and without amplification; which proves that the coherence and the relative phase delay are well preserved through the amplification in SCF.

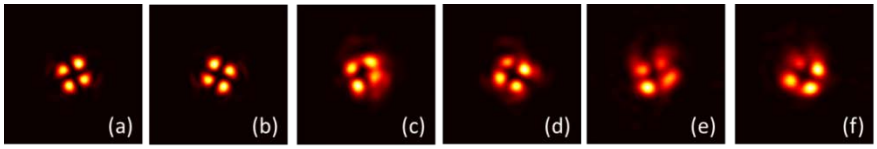

Figure 37 - Coherently combined seeds at far-field with 0 or π phase delay. (a) and (b), simulated; (c) and (d), experimental output with no pump; (e) and (f), with 11 W pump power.

In summary, the excitation and amplification of HOMs in a square-shaped, unclad Ho:YAG SCF has been demonstrated, both with simulation and experiment. Although the incident beam generated using a binary diffraction phase plate cannot match the targeted HOM perfectly, a relatively high modal quality can be achieved and maintained through the amplification process with limited modal degradation. These results will open up applications related to the mode control and amplification of rare earth element doped SCF. The experimental results are undergoing preparation for submitting to a journal for publication.

Students and staff Involved:

1. Dr. Yuan Li – Graduated at 2016, Dec. (PhD) Current Postdoc.
2. Dr. Indumathi Raghu –graduated at 2017, May. (PhD)

3. Dr. Keith Miller – Research Associate
4. Zeyu Zhang, undergraduate student, graduated at 2015, May.
5. Ian Buckley, undergraduate student, graduated at 2015, May.

Publication List

- Yuan Li's PhD dissertation: "Study on the Amplification of Spatial Modes in a Crystal Rod Amplifier", 2016 Dec., Clemson University.

Journal publications

1. Li, Yuan, Keith Miller, Eric G. Johnson, Craig D. Nie, Subhabrata Bera, James A. Harrington, and Ramesh Shori. "Lasing characteristics of Ho: YAG single crystal fiber." Optics Express 24, no. 9 (2016): 9751-9756.
2. Yuan Li, Wenzhe Li, Zeyu Zhang, Keith Miller, Ramesh Shori, and Eric G. Johnson. "Concentric vortex beam amplification: experiment and simulation." Optics Express 24, no. 2 (2016): 1658-1667.
3. Yuan Li, Wenzhe Li, Keith Miller and Eric. G. Johnson, "Multiplexing and Amplification of 2-μmVortex Beams With a Ho:YAG Rod Amplifier," in IEEE Photonics Technology Letters, vol. 28, no. 19, pp. 2031-2034, Oct.1, 1 2016.
4. Y. Li, E. G. Johnson, C. D. Nie, J. A. Harrington, and R. Shori, "Ho:YAG single crystal fiber: fabrication and optical characterization," Opt. Express vol. 22, no. 12, 14896-14903, 2014.

Conference publications

1. Yuan Li, Wenzhe Li, J. Keith Miller, Eric G. Johnson, Subhabrata Bera, Craig Nie, James A. Harrington, "Simultaneous high order modes amplification in Ho:YAG single crystal fiber", accepted to CLEO 2018.
2. Yuan Li, Wenzhe Li, Keith Miller, Eric Johnson, Craig Nie, and James A. Harrington, "Selective Spatial Mode Excitation and Amplification in Ho:YAG Single Crystal Fiber," in Conference on Lasers and Electro-Optics 2017, paper STu4O.4.
3. Yuan Li, Wenzhe Li, Keith Miller, and Eric Johnson, "Multiplexing and Amplification of 2 μm Vortex Beams," in Frontiers in Optics 2016, paper JTh2A.193.
4. Yuan Li, Wenzhe Li, Keith Miller, and Eric Johnson, " Pump Beam Engineering for Vortex Beam in a Ho:YAG Rod Amplifier," in Advanced Solid State Lasers 2016, paper AM5A. 9.
5. Keith Miller, Yuan Li, Wenzhe Li, Ramesh Shori, and Eric Johnson. "Pulsed Amplification of 2 μm Concentric Vortex Beams." In CLEO: Science and Innovations, pp. STu1M-7. Optical Society of America, 2016.

6. Yuan Li, Keith Miller, Eric Johnson, Craig Nie, Subhabrata Bera, James Harrington, and Ramesh Shori. "Ho: YAG Single Crystal Fiber Laser." In Specialty Optical Fibers, pp. SoM4F-2. Optical Society of America, 2016.
7. Yuan Li, Zeyu Zhang, Wenzhe Li, Keith Miller, and Eric Johnson, "Ho:YAG Rod Amplifier For High Order Vortex Modes," in Frontiers in Optics 2015, OSA Technical Digest (Optical Society of America, 2015), paper FTu3G.3.
8. Yuan Li, Zeyu Zhang, Wenzhe Li, Keith Miller, and Eric Johnson, "Simultaneous Amplification of Multiple 2 μm Vortex Beams," in Advanced Solid State Lasers, OSA Technical Digest (online) (Optical Society of America, 2015), paper ATu2A.45.
9. Yuan Li, Zeyu Zhang, J. Keith Miller, and Eric Johnson. "Ho: YAG rod amplifier for vortex beams." In Photonics Conference (IPC), 2015, pp. 321-322. IEEE, 2015.
10. Y. Li, Z. Y. Zhang, I. Buckley, J. K. Miller, E. G. Johnson, C. D. Nie, J. A. Harrington, and R. K. Shori. "Investigation of the amplification properties of Ho: YAG single crystal fiber." In SPIE LASE, pp. 934205-934205. International Society for Optics and Photonics, 2015.

References to Clemson work in Section 5 above:

1. Yuan Li, Wenzhe Li, Keith Miller, and Eric Johnson, "Multiplexing and Amplification of 2 μm Vortex Beams," in Frontiers in Optics 2016, paper JTh2A.193.
2. Yuan Li, Wenzhe Li, Keith Miller, and Eric Johnson, " Pump Beam Engineering for Vortex Beam in a Ho:YAG Rod Amplifier," in Advanced Solid State Lasers 2016, paper AM5A. 9.
3. Yuan Li, Wenzhe Li, Keith Miller, Eric Johnson, Craig Nie, and James A. Harrington, "Selective Spatial Mode Excitation and Amplification in Ho:YAG Single Crystal Fiber," in Conference on Lasers and Electro-Optics 2017, paper STu4O.4.

The Rutgers students involved in this project are:

1. Craig Nie – senior Ph.D. student, graduated Jan, 2017.
2. Subhabrata Bera – Ph.D. student, plans to graduate Mar, 2018.
3. Harry Charalambous – Ph.D. student, completed first year.
4. Michael Soskind – undergraduate student

The University of Michigan students involved in this project are:

1. Stephen Trembath-Reichert
2. Long Cheng
3. Christopher Hoef

The Clemson University students involved in this project are:

1. Yuan Li
2. Indumathi Raghu

Summary of most important results

1. Grew SC fibers from rare-earth doped oxides using the technique of laser heated pedestal growth (LHPG). SC fibers grown to date include Er^{3+}, Ho^{3+}, Yb, and Tm^{3+} doped YAG in diameters from 100 to 300 microns and lengths up to 100 cm.
2. Major improvements were made in the LHPG apparatus mostly through the use of a double transmission axicon system in contrast to the reflective system used by most investigators.
3. An important part of this research is cladding the YAG fibers. We have used the rod-in-tube method to grow SC fibers with a pure YAG clad surrounding an Er:YAG core. The index profiling measurements of this rod-in-tube method indicate that there is a gradient in the Er-ion concentrations with more Er ions in the center than at the edge. These results offer a promising path to producing clad fibers as the fiber is grown in contrast to alternative post-cladding methods.
4. A new method of introducing rare-earth dopants into YAG fiber was developed; This method involved using sol-gel coatings containing rare-earth dopants that were applied to the 330-micron diameter fiber and then regrown into smaller diameters.
5. Lowered the total loss in the pure and doped to less than 0.1 dB/m. This is a 10-fold decrease in loss from a year ago. It is also to our knowledge the lowest loss measured for any SC YAG fiber.
6. Fluorescence measurements of the YAG clad/Er:YAG SC fibers have been made and correlated with the index profiling data of these fibers.
7. The spontaneous emission spectra of 0.5% Er:YAG, 0.5% Ho:YAG fibers have been obtained and the potential pumping wavelengths and laser lines identified.
8. Small signal gain measurements were performed, demonstrating the fiber-like characteristics of the SC fibers.
9. Lasing in 0.5% Ho:YAG SC fibers was obtained from a 11-cm long 330-micron diameter fiber. The slope efficiency of 72.3% is the highest slope efficiency ever obtained for a RE-doped SC fiber. See Ref. 15 for summary of this work.

References

1. T. A. Parthasarathy, R. S. Hay, G. Fair, and F. K. Hopkins, "Predicted performance limits of yttrium aluminum garnet fiber lasers," Opt. Eng. **49**, 094302-1-094302-8 (2010).

2. C. D. Nie, S. Bera, and J. A. Harrington, "Growth of single-crystal YAG fiber optics," Opt. Exp. **24**, 15522-15527 (2016).

3. H. E. LaBelle, "EFG, the invention and application to sapphire growth," J. Cryst. Growth **50**, 8-17 (1980).

4. T. Fukuda and V. I. Chani, *Shaped Crystals-Growth by Micro-Pulling-Down Technique*, (Springer, 2007).

5. Haggerty, J. S., Menashi, W. P., and Wenekkus, J. F. Method for forming refractory fibers by laser energy. US Patent 3,944,640, 3-16-1976.

6. D. H. Jundt, M. M. Fejer, and R. L. Byer, "Growth of optical quality sapphire single crystal fibers," in *Optical Fiber Materials and Processing Symposium 27-29 Nov. 1989 Boston, MA, USA*, J. W. Fleming, G. H. Sigel, Jr., S. Takahashi, and P. W. France, eds., (Pittsburgh, PA, USA, 1990), pp. xiii+357-xiii+358.

7. R. S. F. Chang, V. Phomsakha, and N. Djeu, "Recent advances in sapphire fibers," J. A. Harrington, D. M. Harris, and A. Katzir, eds., Proc. SPIE, **2396**, 1995, pp. 48-53.

8. G. Maxwell, N. Soleimani, B. Ponting, and E. Gebremichael, "Coilable single crystal fibers of doped-YAG for high power laser applications," Proc. SPIE, **8733**, 2013, pp. 87330-1-87330-8.

9. D. J. Gibson and J. A. Harrington, "Extrusion of hollow waveguide preforms with a one-dimensional photonic bandgap structure," J. Appl. Phys. **95**, 3895-3900 (2004).

10. R. Nubling and J. A. Harrington, "Optical properties of single-crystal sapphire fibers," Appl. Opt. **36**, 5934-5940 (1997).

11. R. Nubling and J. A. Harrington, "Single-crystal LHPG sapphire fibers for Er:YAG laser power delivery," Appl. Opt. **37**, 4777-4781 (1998).

12. Dubnikova, N., et al., Sol–gel synthesis and characterization of sub-microsized lanthanide (Ho, Tm, Yb, Lu) aluminium garnets. Optical Materials, 2011. 33(8): p. 1179-1184.

13. J. Sharp, R. Illingworth, and I. Ruddock, "Graded-index characteristics in single-crystal fibers," Optics letters 23, 109-110 (1998).

14. C. D. Nie, S. Bera, J. Melzer, J. A. Harrington, E. Dreyer, S. C. Rand, R. S. Trembath, and C. Hoef, "Erbium distribution in single crystal YAG fibers grown by laser-heated pedestal growth technique," Proc. SPIE, **9342**, 2015, pp. 934204-934209.

15. Y. Li, J. K. Miller, E. G. Johnson, C. D. Nie, S. Bera, J. A. Harrington, and R. Shori, "Lasing characteristics of Ho:YAG single crystal fiber," Opt. Exp. **24**, 9751-9756 (2016).